The Astronomical Journal, 158:182 (17pp), 2019 November https://doi.org/10.3847/1538-3881/ab3ebe

Spectroscopic Follow-up of Discoveries from the NEOWISE Proper Motion Survey

Jennifer J. Greco[1], Adam C. Schneider[2], Michael C. Cushing[1], J. Davy Kirkpatrick[3], and Adam J. Burgasser[4]
[1] Department of Physics and Astronomy, The University of Toledo, Toledo, OH 43606, USA; Jennifer.Greco@rockets.utoledo.edu
[2] School of Earth and Space Exploration, Arizona State University, Tempe, AZ 85282, USA
[3] IPAC, MS 100-22, Caltech, 1200 East California Boulevard, Pasadena, CA 91125, USA
[4] Center for Astrophysics and Space Science, University of California San Diego, La Jolla, CA 92093, USA
Received 2019 June 28; revised 2019 August 23; accepted 2019 August 23; published 2019 October 14

Abstract

We present low-resolution near-infrared spectra of discoveries from an all-sky proper motion search conducted using multi-epoch data from the *Wide-field Infrared Survey Explorer*. Using the data from NEOWISE, along with the AllWISE catalog, Schneider et al. conducted an all-sky proper motion survey to search for nearby objects with high proper motions. Here, we present a follow-up spectroscopic survey of 65 of their discoveries, which focused primarily on potentially nearby objects ($d < 25$ pc), candidate late-type brown dwarfs ($\geqslant$L7), and subdwarf candidates. We found 31 new M dwarfs, 18 new L dwarfs, and 11 new T dwarfs. Of these, 13 are subdwarfs, including one new sdL1 and two new sdL7s. Eleven of these discoveries, with spectral types ranging from M7 to T7 (including one subdwarf) are predicted to be within 25 pc, adding to the number of known objects in the solar neighborhood. We also discovered three new early-type T subdwarf candidates, one sdT1, one sdT2, and one sdT3, which would increase the number of known early-type T subdwarfs from two to five.

Unified Astronomy Thesaurus concepts: Brown dwarfs (185); L dwarfs (894); T dwarfs (1679); M dwarf stars (982); L subdwarfs (896); T subdwarfs (1680); M subdwarf stars (986); Low mass stars (2050); Spectroscopy (1558); Infrared astronomy (786)

Supporting material: data behind figures

1. Introduction

The census of stars and brown dwarfs in the solar neighborhood expanded dramatically with the launch of the *Wide-field Infrared Survey Explorer* (*WISE*; Wright et al. 2010). Discoveries include the third and fourth closest systems to the Sun in WISE J104915.57−531906.1AB (hereafter WISE 1049−5319AB; Luhman 2013) and WISE J085510.83−071442.5 (hereafter WISE 0855−0714; Luhman 2014a), a substantial increase in the number of known late-type T dwarfs (e.g., Mace et al. 2013), a new spectral class (Y dwarfs; Cushing et al. 2011; Kirkpatrick et al. 2012), and the M9 dwarf, WISE J072003.20−084651.2, located in the Galactic plane (hereafter WISE 0720−0846; Kirkpatrick et al. 2014; Scholz 2014). WISE 0720−0846, which is an M9.5/T5 binary (Burgasser et al. 2015) at a distance of 6.72 ± 0.05 pc (Henry et al. 2018), is of particular interest because it passed within $0.25^{+0.11}_{-0.07}$ pc of the Sun 70 ky ago, in the closest known flyby of a star to the solar system (Mamajek et al. 2015).

WISE was built to survey the entire sky simultaneously in four mid-infrared bands whose central wavelengths are at 3.4 μm (*W*1), 4.6 μm (*W*2), 12 μm (*W*3), and 22 μm (*W*4). The four-band cryogenic mission surveyed the sky 1.2 times between 2010 January and August. After the cryogen in the outer tank was depleted, a three-band cryogenic survey was conducted using the *W*1, *W*2, and *W*3 bands, covering an additional 30% of the sky, until the cryogen in the inner tank was also exhausted in 2010 September. Following this, a two-band survey was conducted using only the *W*1 and *W*2 bands (Mainzer et al. 2011). The result of these surveys was two full maps of the sky and 20% of a third, separated by ∼6 months. The data from all of these surveys were combined and used to generate the AllWISE source catalog (Cutri 2014). The *WISE* satellite was then put into hibernation until 2013 December, when it was reactivated to search for potentially hazardous near-Earth objects, using the *W*1 and *W*2 bands alone (NEOWISE; Mainzer et al. 2014).

The multi-epoch nature of the *WISE* observations meant that for the first time, all-sky proper motion surveys at infrared wavelengths were possible. Luhman (2014b) and Kirkpatrick et al. (2014, 2016) used the data from the original *WISE* mission with a time baseline of ∼6 months to perform the first all-sky mid-infrared proper motion searches, finding 762, 3525, and 1039 new discoveries, respectively. Schneider et al. (2016) used the NEOWISE data in combination with the AllWISE source catalog to conduct a proper motion survey with a time baseline of ∼4 yr. The longer time baseline of their survey enabled them to detect significantly more objects at fainter magnitudes than the surveys of Luhman (2014b) and Kirkpatrick et al. (2014); (see Figure 8 of Schneider et al. 2016).

The Schneider et al. (2016) survey discovered 20,551 motion objects, of which 1006 were new discoveries. In this paper, we present follow-up observations of 65 of these new discoveries. In Section 2, we describe how we selected our targets for follow-up observations. In Section 3, we detail the follow-up observations that were conducted and present all of our follow-up spectra. In Section 4, we present spectral types and distance estimates for each of our objects. In Section 5, we discuss our follow-up observations in detail.

2. Target Selection

In order to prioritize follow-up spectroscopic observations, Schneider et al. (2016) identified 128 objects that fell into at least one of three categories: (1) potential late-type brown dwarfs (spectral type $\geqslant$L7), (2) potential nearby objects ($d < 25$ pc), and (3) potential subdwarfs (i.e., low metallicity

Table 1
Summary of Observations

AllWISE Designation[a]	UT Date	Telescope/Instrument	Total Exp Time(s)	A0 V Star	S/N[b]
J000430.66−260402.3	2016 Aug 3	IRTF/SpeX	2151	HD 225200	45
J000458.47−133655.1	2016 Sep 22	IRTF/SpeX	2151	HD 1154	18
J000536.63−263311.8	2016 Sep 22	IRTF/SpeX	2151	HD 222332	19
J000856.39−281321.7	2016 Sep 21	IRTF/SpeX	2151	HD 225200	18
J010134.83+033616.0	2016 Sep 22	IRTF/SpeX	1434	HD 6457	81
J010631.20−231415.1	2016 Sep 21	IRTF/SpeX	2151	HD 13433	12
J011049.18+192000.1	2016 Oct 24	IRTF/SpeX	1434	HD 6457	46
J013525.38+020518.2	2016 Aug 6	IRTF/SpeX	2151	HD 1154	22
J022721.93+235654.3	2016 Aug 3	IRTF/SpeX	2151	HD 13869	38
J030119.39−231921.1	2016 Aug 3	IRTF/SpeX	1912	HD 19622	28
J030919.70−501614.2	2016 Jul 18	*Magellan*/FIRE	1374	HD 8811	43
J031627.79+265027.5	2016 Aug 6	IRTF/SpeX	2151	HD 19600	35
J032309.12−590751.0	2016 Jul 18	*Magellan*/FIRE	1374	HD 325	64
J032838.73+015517.7	2016 Aug 6	IRTF/SpeX	2151	HD 18571	24
J033346.88+385152.6	2016 Sep 21	IRTF/SpeX	1673	HD 21038	51
J034409.71+013641.5	2016 Sep 21	IRTF/SpeX	2151	HD 21686	14
J034858.75−562017.8	2016 Jul 18	*Magellan*/FIRE	1099	HD 325	24
J041353.96−202320.3	2017 Jan 16	IRTF/SpeX	1673	HD 25754	25
J041743.13+241506.3	2016 Feb 24	IRTF/SpeX	2151	HD 25175	62
J053424.45+165255.0	2016 Feb 24	IRTF/SpeX	1434	HD 35036	97
J054455.54+063940.3	2016 Sep 21	IRTF/SpeX	1434	HD 35153	158
J061429.77+383337.5	2016 Feb 24	IRTF/SpeX	717	HD 45105	270
J062858.69+345249.2	2016 Feb 24	IRTF/SpeX	1434	HD 45105	48
J063552.52+514820.4	2017 Nov 22	IRTF/SpeX	714	HD 45105	16
J084254.56−061023.7	2016 Feb 24	IRTF/SpeX	2151	HD 63714	69
J085039.11−022154.3	2016 Feb 24	IRTF/SpeX	1434	HD 79108	89
J085633.87−181546.6	2016 Mar 28	IRTF/SpeX	1434	HD 82724	45
J092453.76+072306.0	2016 Feb 24	IRTF/SpeX	1434	HD 79108	67
J094812.21−290329.5	2016 Feb 24	IRTF/SpeX	1434	HD 94741	60
J095230.79−282842.2	2016 Feb 24	IRTF/SpeX	1434	HD 81694	96
J101944.62−391151.6	2016 Dec 9	CTIO/ARCoIRIS	2880	HD 89213	19
J103534.63−071148.2	2016 Mar 28	IRTF/SpeX	2151	HD 93346	35
J111320.39+501010.5	2016 Mar 28	IRTF/SpeX	1434	HD 99966	85
J112158.76+004412.3	2016 Feb 24	IRTF/SpeX	1434	HD 97585	43
J112859.45+511016.8	2016 Mar 28	IRTF/SpeX	1434	HD 99966	42
J120751.17+302808.9	2016 Feb 24	IRTF/SpeX	1434	HD 105388	121
J121231.97−050750.7	2016 Mar 28	IRTF/SpeX	1434	HD 109309	117
J121914.75+081027.0	2016 Feb 24	IRTF/SpeX	1434	HD 116960	60
J122042.20+620528.3	2016 Jun 20	IRTF/SpeX	1434	HD 148968	44
J123513.87−045146.5	2016 Jun 26	IRTF/SpeX	2151	HD 109309	41
J124516.66+601607.5	2016 Feb 24	IRTF/SpeX	1434	HD 118214	79
J133520.09−070849.3	2016 May 10	IRTF/SpeX	1434	HD 122749	19
J134359.71+634213.1	2016 May 10	IRTF/SpeX	1434	HD 118214	31
J143942.79−110045.4	2016 Feb 24	IRTF/SpeX	1673	HD 136831	66
J144056.64−222517.8	2016 Jun 20	IRTF/SpeX	1434	HD 133466	106
J145645.54−103343.5	2016 Mar 28	IRTF/SpeX	1434	HD 132072	78
J145747.55−094719.3	2016 Mar 28	IRTF/SpeX	1434	HD 132072	56
J155225.22+095155.5	2016 Jun 20	IRTF/SpeX	1434	HD 136831	70
J165057.66−221616.8	2016 May 10	IRTF/SpeX	717	HD 155379	291
J171059.52−180108.7	2016 May 10	IRTF/SpeX	717	HD 154921	279
J171105.08−275531.7	2016 May 10	IRTF/SpeX	717	HD 157918	220
J171454.88+064349.8	2016 Mar 28	IRTF/SpeX	1912	HD 161289	42
J173551.56−820900.3	2016 Jul 18	*Magellan*/FIRE	1374	HD 131912	89
J180839.55+070021.7	2016 May 10	IRTF/SpeX	2151	HD 167163	32
J182010.20+202125.8	2016 Oct 24	IRTF/SpeX	1434	HD 171623	8
J183654.10−135926.2	2016 Oct 24	IRTF/SpeX	1075	HD 172904	13
J191011.03+563429.3	2016 Jun 20	IRTF/SpeX	717	HD 172728	317
J201252.78+124633.3	2016 Sep 22	IRTF/SpeX	1195	HD 191082	533
J211157.84−521111.3	2016 Jul 18	*Magellan*/FIRE	1374	HD 200523	63
J215550.34−195428.4	2016 Oct 14	IRTF/SpeX	1912	HD 203893	10
J221737.41−355242.7	2016 Oct 24	IRTF/SpeX	2151	HD 202941	13

Table 1
(Continued)

AllWISE Designation[a]	UT Date	Telescope/Instrument	Total Exp Time(s)	A0 V Star	S/N[b]
J223444.44−230916.1	2016 Oct 14	IRTF/SpeX	2151	HD 212643	7
J224931.10−162759.6	2016 Oct 14	IRTF/SpeX	2151	HD 212643	24
J230743.63+052037.3	2016 Oct 24	IRTF/SpeX	1434	HD 219833	54
J234404.85−250042.2	2016 Sep 22	IRTF/SpeX	1434	HD 225200	81

Notes.
[a] The prefix for AllWISE sources is WISEA. So for example J000430.66−260402.3 should be listed as WISEA J000430.66−260402.3.
[b] Calculated at the peak intensity in the *J*-band.

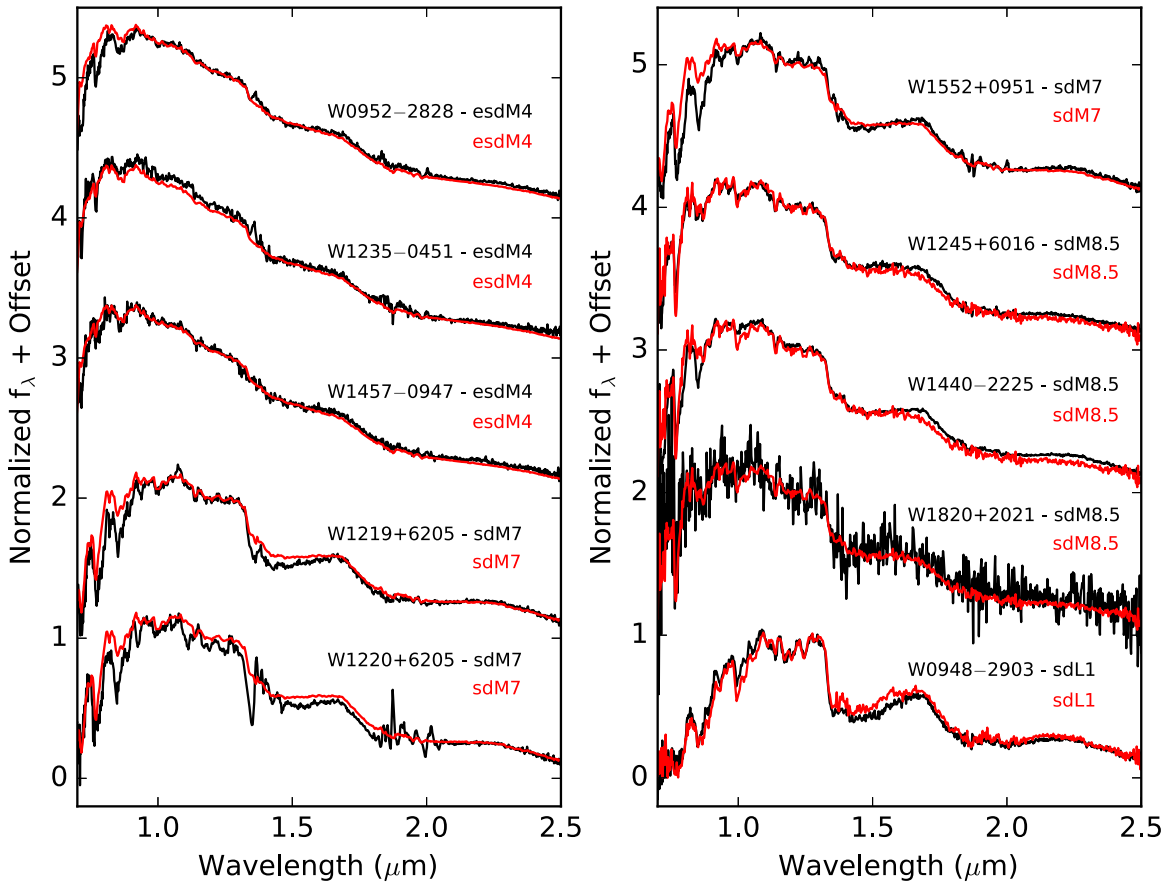

Figure 1. Spectra of all observed objects, plotted against the appropriate spectral standards.
(The data used to create this figure are available.)

dwarfs). To begin their candidate selection, Schneider et al. (2016) first estimated the spectral types of their new discoveries using available near- and mid-infrared photometry and the k-nearest neighbors method against a training set of objects with known spectral types (see Appendix A of Schneider et al. 2016 for details). They identified a total of 39 candidates with estimated spectral types later than or equal to L7 and presented spectroscopy of six of these. Distances to all new discoveries were then computed using the photometric-based spectral types, *W*2 magnitudes, and the absolute magnitude–spectral type relations of Dupuy & Liu (2012). They identified a total of 46 objects with distance estimates less than or equal to 25 pc and presented spectroscopy of three of these. Finally, a total of 58 potential subdwarfs were identified using both a color cut and a reduced proper motion diagram, and spectroscopy of six of these were presented.

Here we present near-infrared spectroscopy of 65 additional objects. Of these, 53 were selected from the 128 sources selected by Schneider et al. (2016): 23 candidate late-type brown dwarfs, 21 potentially nearby objects, and 21 subdwarf candidates. Eleven of these were candidates in more than one category, including WISE J032309.12−590751.0 and WISE J101944.62−391151.6, which were candidates in all three categories. Three additional objects, WISE J111320.39+501010.5, WISE J121231.97−050750.7, and WISE J145747.55−094719.3, were identified as subdwarf candidates early on in the survey based on their high tangential velocities ($v_{\rm tan} > 100$ km s^{-1}). During gaps in our R.A. coverage, we supplemented our target list with

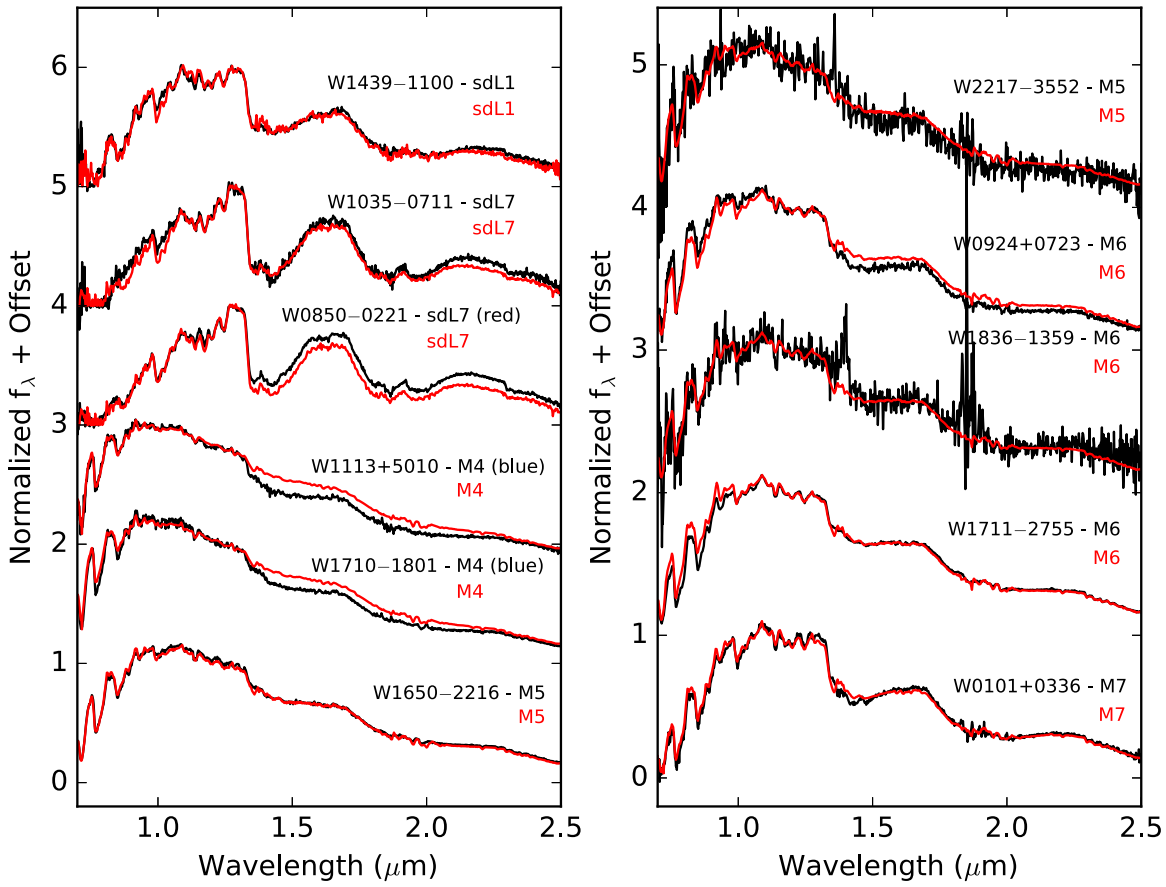

Figure 2. Spectra of all observed objects, plotted against the appropriate spectral standards.
(The data used to create this figure are available.)

additional mid-L candidates, observing a total of seven additional objects. Finally, on one night with particularly poor weather, we observed two bright M-dwarf candidates.

3. Observations

A summary of all follow-up observations is provided in Table 1. Included in this table are the AllWISE designation for each object (hereafter these will be abbreviated as WISE HHMM–DDMM), the UT date of the observation, the telescope/instrument used to conduct the observations, the total exposure time used for each spectrum, the signal-to-noise of the resultant spectra calculated at the peak intensity in the *J*-band, and the A0 V star observed for calibration purposes. All spectra are plotted in Figures 1–6, sorted by spectral type.

3.1. IRTF/SpeX

Spectra of 59 objects were obtained using the SpeX spectrograph (Rayner et al. 2003) on the NASA Infrared Telescope Facility (IRTF) on Mauna Kea. Observations were conducted between the dates of UT 2016 February 24 and UT 2017 November 22 (see Table 1 for full list of observation dates). The data were collected in prism mode spanning a wavelength range of 0.8–2.5 μm with a resolution of $R \equiv \lambda/\triangle\lambda = 250$, using either the 0.″5-wide slit or the 0.″3-wide slit aligned to the parallactic angle. For each object, a series of exposures were taken using an ABBA nod pattern along the 15″ long slit. Additionally, an A0 V star was observed at a similar airmass to each object and used for telluric correction and flux calibration. The data were all reduced using the Spextool package (Vacca et al. 2003; Cushing et al. 2004).

In order to determine the spectral type of our subdwarf candidates, we require spectra of subdwarf standards. One of us (A.J.B) obtained spectra of 16 M and L subdwarf standards using IRTF/SpeX. Observations were conducted between the dates of UT 2003 September 17 and UT 2006 December 21. Data were collected in prism mode, as discussed above, and reduced using the Spextool package (Vacca et al. 2003; Cushing et al. 2004). A list of these standards, their spectral types, the references for those spectral types, and the details of those observations are listed in Table 2. Spectra of these objects are shown in Figure 7.

3.2. Magellan/FIRE

Spectra of five objects were obtained with the Folded-Port Infrared Echellete (FIRE; Simcoe et al. 2013) spectrograph on the *Magellan* 6.5 m Baade Telescope at Las Campanas Observatory. Observations were conducted on UT 2016 July 18. All observations were made with the high-throughput prism mode, which achieved a resolving power of $R \sim 450$ across the 0.8–2.45 μm range. We used the 0.″6-wide slit, aligned to the parallactic angle, and took exposures at two different nod positions along the slit. For all science targets,

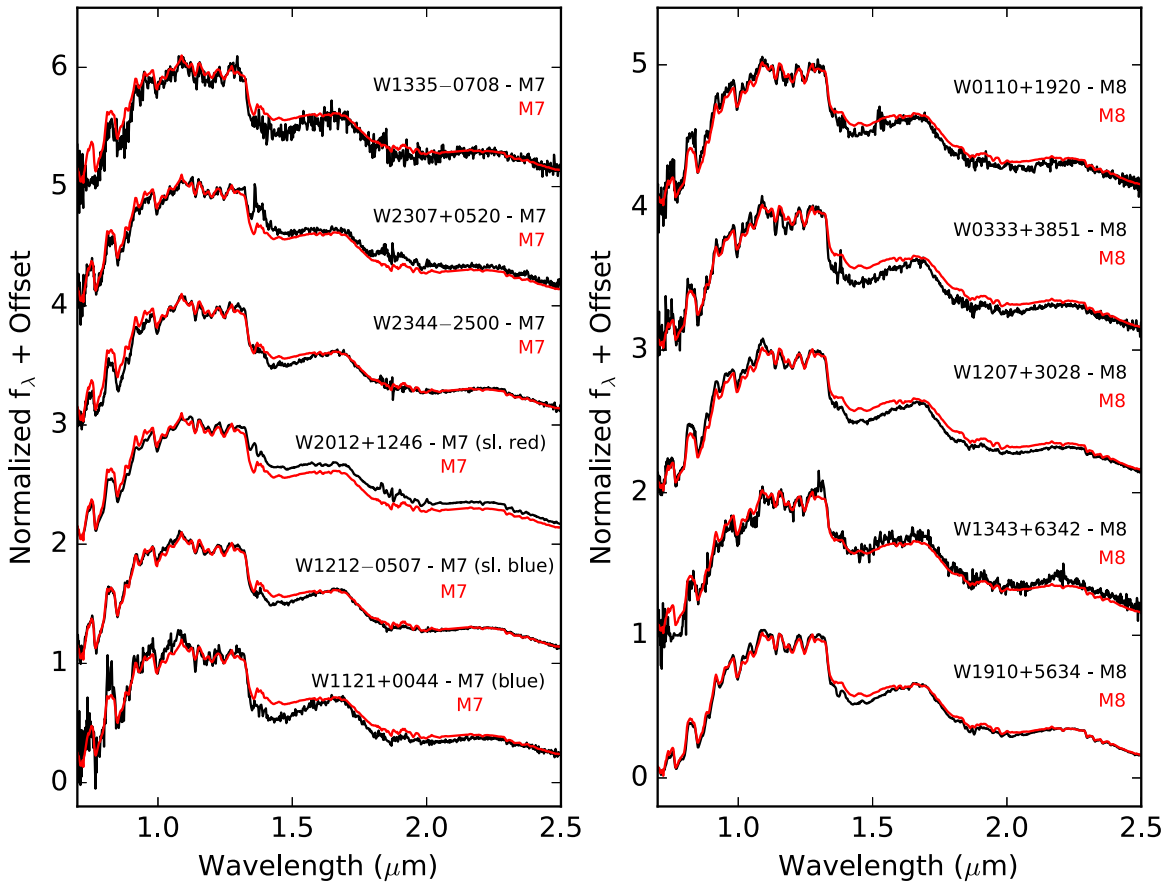

Figure 3. Spectra of all observed objects, plotted against the appropriate spectral standards.
(The data used to create this figure are available.)

the sample-up-the-ramp mode was used. A0 V stars were observed after each science target to correct for telluric absorption and flux calibration. Data reduction was performed using a modified version of the Spextool reduction package (Vacca et al. 2003; Cushing et al. 2004).

3.3. CTIO/ARCoIRIS

One object was observed on UT 2016 December 9 with Astronomy Research using the Cornell Infrared Imaging Spectrograph (ARCoIRIS) on the 4 m Blanco telescope located at the Cerro Tolo Inter-American Observatory (CTIO). ARCoIRIS takes simultaneous spectra across six cross-dispersed orders covering the 0.8–2.4 μm range, with a resolving power of ∼3500. Science exposures were taken at two different nod positions along the slit, which has a fixed width of 1″. After observing our science target, we observed an A0 V star to use for telluric corrections and flux calibration. Data reduction was performed using a modified version of the Spextool reduction package (Vacca et al. 2003; Cushing et al. 2004).

4. Results

4.1. Spectral Classification

Spectral types were determined by comparing each spectrum to the near-infrared spectral standards from Kirkpatrick et al. (2010) and the near-infrared M and L subdwarf standards given in Table 2. First, the standard and object spectra were normalized to unity between 1.27 and 1.29 μm. One of us (J.J.G.) then assigned spectral types by eye, based on which spectral standard was the best match to each object over the 0.9–1.4 μm wavelength range. Some spectra fall appreciably red or blue of the spectral standards in the *H*- and *K*-bands and these are typed as red or blue, respectively. Another one of us (A.C.S.) confirmed all spectral types by eye, and the results are listed in Table 3.

In total, we present spectra of 31 new M dwarfs, 18 new L dwarfs, and 11 new T dwarfs. Spectra of one additional L dwarf and four additional T dwarfs are also presented, but these have been previously published as discussed below. Thirteen of our objects are subdwarfs, including nine new M subdwarfs and four new L subdwarfs. Eleven of these objects (including two subdwarfs) with spectral types ranging from M7 to T7 are predicted to be within 25 pc.

Five of our 65 objects have previously published spectra. Best et al. (2015) published a spectrum of WISE 0135+0205 (PSO J023.8557+02.0884), classifying it as an L9.5. We classified it as T0 (sl. red). Best et al. (2015) observed WISE 0316+2650 (PSO J049.1159+26.8409), classifying it as T2.5, with strong potential of being a binary. We classified it as a T3. Tinney et al. (2018) published a spectrum of WISE 1735 −8209, classifying it as a T8; we classify it as a T7. Luhman & Sheppard (2014) observed WISE 2111−5211, classifying it as a T2.5; we typed it as a T3. Best et al. (2015) observed WISE 2249−1627 (PSO J342.3797−16.4665), classifying it as an L5, possibly in a binary with a T dwarf. Robert et al. (2016)

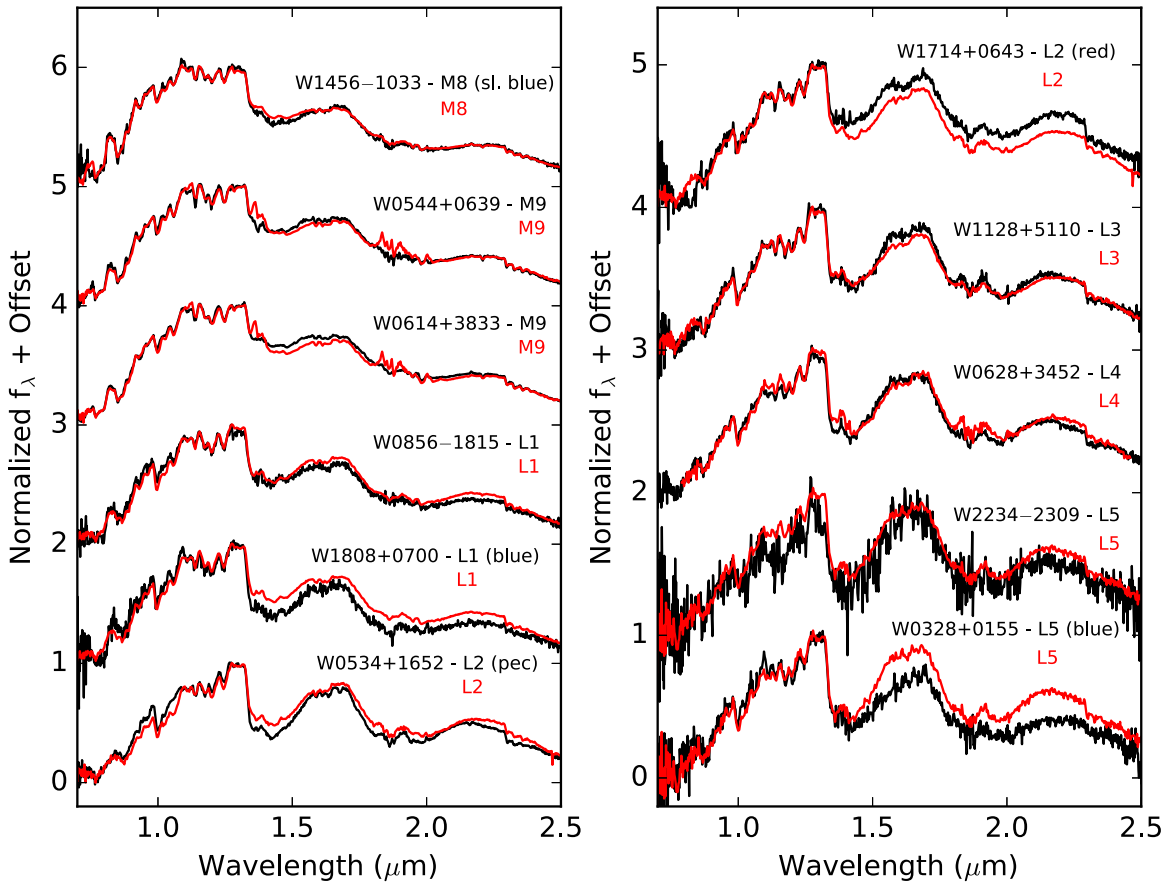

Figure 4. Spectra of all observed objects, plotted against the appropriate spectral standards.
(The data used to create this figure are available.)

also observed this object, classifying it as an L4/T1 binary. We classified this as an L5 (blue).

Additionally, two objects have published spectral types estimated using photometry. Tinney et al. (2018) used methane imaging to spectral type WISE 0309−5016 as a T7, which agrees with our spectral type. Kirkpatrick et al. (2019) note that, because this object is much brighter in M_H than other objects of similar $H - W2$ color, and much brighter in M_{W1} and M_{ch1} than other objects of similar *Spitzer* ch1−ch2 color, it is likely an unresolved binary. Kirkpatrick et al. (2019) estimated the spectral type of WISE 0323−5907 based on *Spitzer* ch1 and ch2 photometry to be a T6. We classified this object as a T7.

Finally we note that, in Table 10 of Schneider et al. (2016), the spectral type of WISE 0413+2103 was mistaken for that of WISE 0413−2023. This caused WISE 0413+2103 to be listed as a late-type candidate, when it is in fact an M dwarf. We noticed this while selecting our follow-up candidates, and so observed WISE 0413−2023, which has a spectral type of L5 (blue).

4.2. Distance Estimates

We can improve upon the spectrophotometric distances of Schneider et al. (2016) using available photometry and absolute magnitude–spectral type relations to compute spectroscopic distances for each of our objects. We primarily used the relations of Dupuy & Liu (2012), which are valid for objects with spectral types between M6 and T9 (inclusive) and can be used with Two Micron All Sky Survey (2MASS) J, H, and K_s and *WISE* $W1$ and $W2$ photometry. For spectral types earlier than M6, we used the relations of Zhang et al. (2013), which are valid for spectral types between M1 and L9 (inclusive) and can be used with 2MASS J, H, and K_s photometry. Finally, for the subdwarfs, we used the relations of Zhang et al. (2017), which are valid for subdwarfs with spectral types between M0 and L7 (inclusive) and can be used with 2MASS J- and H-band photometry.

These relations were combined with available photometry to calculate the distances and their uncertainties using a Monte Carlo approach to properly account for the uncertainties in the spectral type, spectral type–absolute magnitude relation, and the photometry. We randomly drew from distributions for the spectral type, the absolute magnitude, and the apparent magnitude to compute a distance. A uniform distribution with a width of 1 subtype centered on the spectral type of the object was used for the spectral type distribution, a normal distribution with a mean and standard deviation given by the spectral type–absolute magnitude relation and rms uncertainty of that relation was used for the absolute magnitude relation, and a normal distribution with a mean and standard deviation given by the apparent magnitude and its uncertainty was used for the apparent magnitude distribution. The process was repeated 10,000 times for each object, and the mean and standard deviation of the resulting distribution gave us the spectroscopic distance and its uncertainty. Distances and

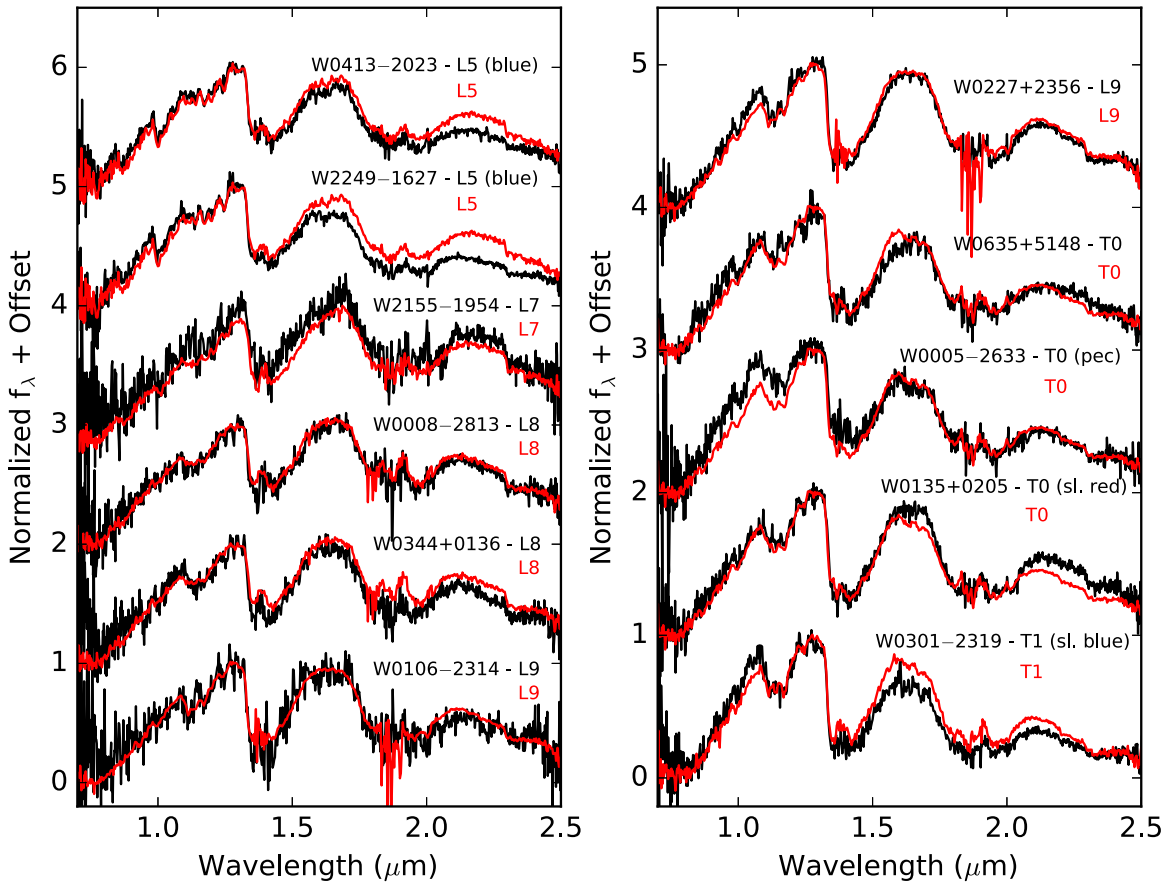

Figure 5. Spectra of all observed objects, plotted against the appropriate spectral standards.
(The data used to create this figure are available.)

uncertainties were calculated for each object in the filters where the spectral type–absolute magnitude relations are valid, and a weighted average of all individual spectroscopic distances for each object was then used to calculate the final spectroscopic distances, which can be found in Table 4.

Most of our distances are within, or close to, the distance ranges from the Schneider et al. (2016) survey. WISE 1710−1801 shows a large discrepancy between the spectroscopic distance calculated in this paper (60 ± 12 pc) and the spectrophotometric distance estimated in Schneider et al. (2016; 24–37 pc). This is likely a result of the fact that Schneider et al. (2016) used the Dupuy & Liu (2012) relations to calculate their distance estimate, and these relations are not valid for early M dwarfs. The estimate in this paper used the Zhang et al. (2013) relations, which are valid for early M dwarfs.

We also searched the *Gaia* DR2 archive to identify which of our candidates were detected by *Gaia*. Using the 2MASS–AllWISE proper motions calculated by Schneider et al. (2016), and the positions of our sources from the AllWISE epoch (2010.5), we calculated the positions of each of our sources in the *Gaia* epoch (2015.5). It was not possible to do this for WISE 0309−5016, because it was not detected in 2MASS and Schneider et al. (2016) were not able to calculate a 2MASS–AllWISE proper motion for it. We then cross-matched the positions of our objects at the *Gaia* epoch against the *Gaia* DR2 archive, and identified all *Gaia* matches within 5″. We then examined all the matches for each object to confirm matches, and in some cases, determine which of the multiple matches was the correct object. This was accomplished by: first, performing a visual inspection of each of our objects using finder charts, examining the position of our object in images from Digitalized Sky Survey (DSS), UKIRT InfraRed Deep Sky Surveys (UKIDSS), 2MASS, *WISE*, and Pan-STARRs, where available. Second, the separation was calculated between the coordinates we calculated for each object at the *Gaia* epoch and the coordinates for each match in the *Gaia* DR2 catalog to determine which of the multiple matches was closest to the coordinates we calculated. Third, we compared the proper motions for each match in the *Gaia* catalog to the proper motions for each source calculated in Schneider et al. (2016) to make sure those values matched.

In total, 32 of our 65 objects have matches in *Gaia*. They are all listed in Table 4, along with the *Gaia* source ID for each match, and the *Gaia* distances for each object (Bailer-Jones et al. 2018). Two of our objects (WISE 0850−0221 and WISE 1808+0700) had matches in the *Gaia* catalog with no parallax measurements, and so are not included in Table 4. For most of our objects, we find good agreement between our spectroscopic distances and the *Gaia* distances, as well as the 2MASS–AllWISE proper motions and the *Gaia* proper motions, as can be seen in Figure 8. For WISE 1113+5010, we noticed a large discrepancy between our spectroscopic distance of 260 ± 31 pc and the *Gaia* distance of $181^{+10.4}_{-9.3}$ pc. Our spectral type for this object is an M4 (blue), meaning it exhibits suppressed flux in the *H*- and *K*-bands, relative to the *J*-band, causing it to

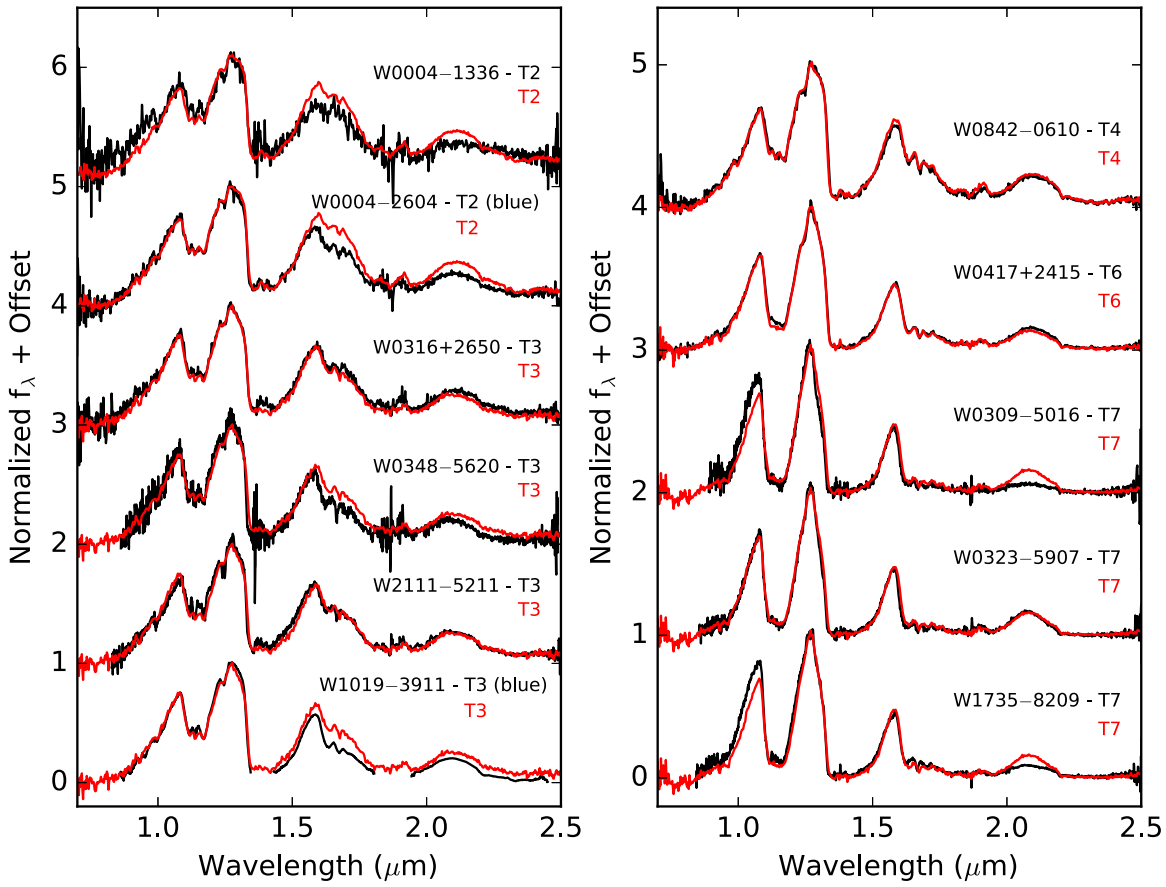

Figure 6. Spectra of all observed objects, plotted against the appropriate spectral standards.
(The data used to create this figure are available.)

appear bluer in the *H*- and *K*-bands than the field objects of the same spectral class. This is typically an indicator that an object could be a subdwarf (this is discussed in greater detail in Section 5.3). If we use the absolute magnitude–spectral type relations for subdwarfs, we get a distance of 140 ± 19 pc, which is much closer to the *Gaia* distance. This suggests that WISE 1113+5010 may either be a subdwarf (sdM4) or an intermediate subdwarf (d/sdM4). Unfortunately, we do not have a spectrum of a sdM4 standard, and so we cannot confirm this hypothesis.

Included in Table 4 along with our *Gaia* distances, are distances for three objects (WISE 0309−5016, WISE 0323−5907, and WISE 1735−8209) calculated from parallaxes obtained by Kirkpatrick et al. (2019) using the Infrared Array Camera (IRAC; Fazio et al. 2004) on the *Spitzer Space Telescope* (Werner et al. 2004). The distances for WISE 0309−5016 and WISE 1735−8209 agree very well with the spectroscopic distances we calculated, but the distance for WISE 0323−5907 does not, as can be seen in Figure 8. The parallax from Kirkpatrick et al. (2019) gives a distance of 14.0 ± 0.84 pc, and our spectroscopic distance is 19 ± 2.1 pc. The reason for the large discrepancy is still unclear. Kirkpatrick et al. estimate the spectral type of this object to be T6, based on the ch1−ch2 photometry but, according to our spectrum from IRTF/SpeX, it is a textbook T7. Kirkpatrick et al. note that this source is too faint in *W*1 and *W*2 for its Spitzer ch1−ch2 color. If we calculate the distance using only the 2MASS *J*-band photometry (which comes from the 2MASS reject catalog), we get a distance of 18.1 ± 4.2 pc, which falls within 1σ of the Kirkpatrick et al. value. This object will need to be studied further to determine the exact reason for this discrepancy.

5. Discussion

5.1. Nearby Objects

Volume-limited samples are the gold standard in astrophysics because they provide an unbiased sample of the objects under scrutiny. Constructing a complete census of the stars and brown dwarfs in the solar neighborhood is particularly important because this region contains the brightest, and thus most easily studied, objects of a given spectral class. At least one star or brown dwarf has been added to the list of stellar systems that lie within 10 pc of the Sun every year since 2002 (Henry et al. 2018) indicating that the local census remains incomplete. The intrinsic faintness of brown dwarfs makes constructing volume-limited samples difficult, particularly out to larger distances where the census is even more incomplete.

Our survey and follow-up observations have identified 21 new objects within 30 pc of the Sun. Eleven of these objects have distances within 25 pc: one M dwarf (WISE 2012+1246 M7; sl. red), nine T dwarfs (WISE 0004−2604 T2 (blue), WISE 0135+0205 T0 (sl. red), WISE 0309−5016 T7, WISE 0316+2650 T3, WISE 0323−5907 T7, WISE 0417+2415 T6, WISE 0842−0610 T4, WISE 1019−3911 T3 (blue), and WISE 1735−8209 T7), and one L subdwarf (WISE 0850−0221 sdL7; red). An additional 10 objects have spectroscopic distances of

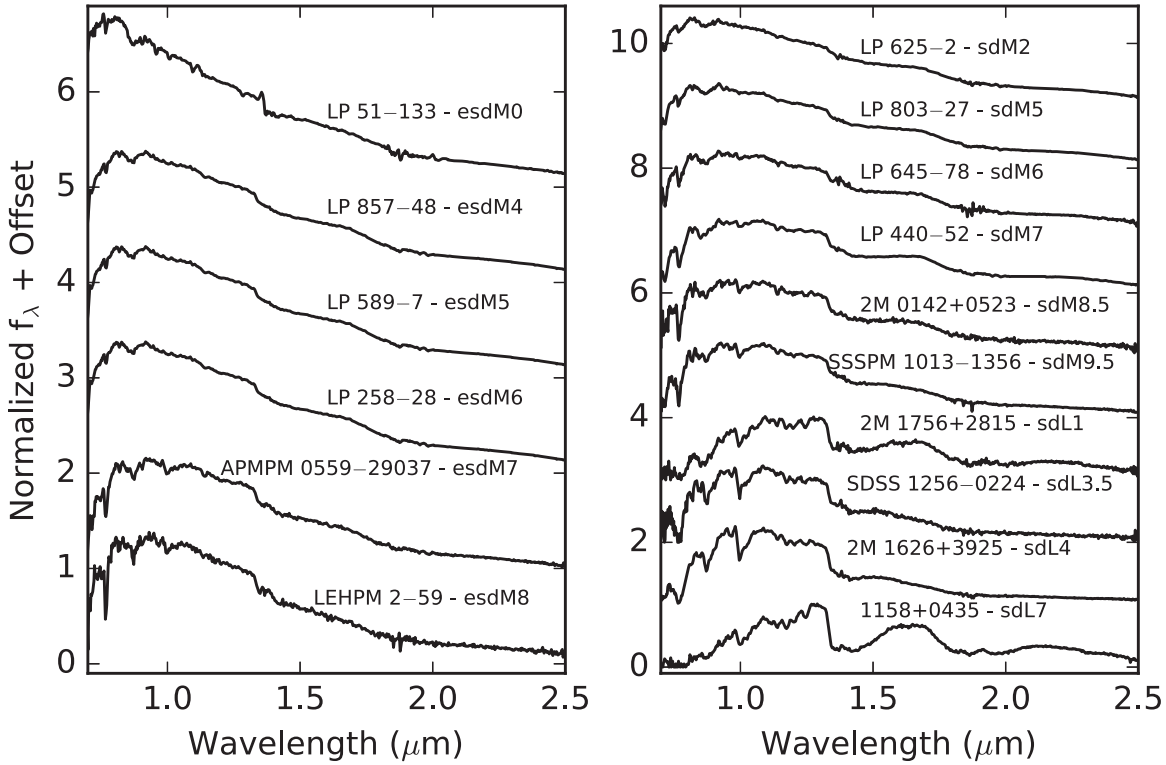

Figure 7. Subdwarf standards, listed in Table 2.
(The data used to create this figure are available.)

Table 2
Subdwarf Standards

Object Name	Other Designation	Optical Spectral Type	Spectral Type Reference	UT Date	Exp Time[a] (s)	A0 V Star[a]	S/N[b]
LP 51−133	LHS 217	esdM0[c]	Kirkpatrick et al. (2010)	2006 Dec 21	320	HD 33654	412
LP 857−48	LHS 375	esdM4	Gizis (1997)	2005 Mar 23	540	HD 125299	318
LP 589−7	⋯	esdM5	Gizis & Reid (1999)	2004 Sep 5	1080	HD 13936	318
LP 258−28	LHS 2023	esdM6	Reid & Gizis (2005)	2005 Mar 23	1080	HD 58729	318
APMPM J0559−29037	⋯	esdM7	Schweitzer et al. (1999)	2005 Dec 31	1440	HD 41473	159
LEHPM 2−59	⋯	esdM8	Burgasser & Kirkpatrick (2006)	2004 Sep 9	720	HD 32855	120
LP 625−2	LHS 3181	sdM2	Riaz et al. (2008)[d]	2004 Jul 25	720	HD 143459	758
LP 803−27	LHS 407	sdM5	Gizis (1997)	2004 Jul 25	480	HD 133772	639
LP 645−78	LHS 1074	sdM6	Reid & Gizis (2005)	2004 Sep 8	1080	HD 18735	173
LP 440−52	LHS 377	sdM7	Gizis (1997)	2004 Mar 12	480	HD131951	514
2MASS J01423153+0523285	⋯	sdM8.5[e]	Burgasser et al. (2007)	2003 Sep 17	720	HD 18571	60
SSSPM J1013−1356	⋯	sdM9.5	Scholz et al. (2004)	2004 Mar 12	720	HD 88025	165
2MASS J17561080+2815238	⋯	sdL1[f]	Kirkpatrick et al. (2010)	2005 Oct 20	960	HD 160557	78
SDSS J125637.13−022452.4	⋯	sdL3.5	Burgasser et al. (2009)	2005 Mar 23	1080	HD 111744	87
2MASS J16262034+3925190	⋯	sdL4	Burgasser et al. (2007)	2004 Jul 23	480	HD 153345	429
SDSS J115820.75+043501.7	⋯	sdL7[g]	Kirkpatrick et al. (2014)	2006 Apr 8	1080	HD 97585	106

Notes.
[a] Exact exposure times and which A0V stars were used could not be determined because the original FITS headers from the reduction were lost. Therefore we estimated the exposure times and standards using the raw data frames obtained form the IRTF Legacy Archive (http://irtfdata.ifa.hawaii.edu/search/).
[b] Calculated at the peak intensity in the *J*-band.
[c] Kirkpatrick et al. (2010) classify this object in the near-infrared as <esdM5.
[d] Riaz et al. (2008) reference Ruiz & Anguita (1993) for the spectral type, which provides a spectrum but no spectral type.
[e] Burgasser et al. (2004) classify this object in the near-infrared as similar to, or slightly later than, sdM7.5.
[f] Kirkpatrick et al. (2010) classify this object in the near-infrared as L1 pec (blue).
[g] Kirkpatrick et al. (2010) classify this object in the near-infrared as sdL7.

Table 3
Spectral Types

AllWISE Designation	Photometric[a] Spectral Type	Spectral Type[b] from Observations	Follow-up[c] Category
J000430.66−260402.3	20.5	T2 (blue)	l
J000458.47−133655.1	16.9	T2	g
J000536.63−263311.8	17.1	T0 (pec)	l
J000856.39−281321.7	18.0	L8	n, l
J010134.83+033616.0	7.0	M7	s
J010631.20−231415.1	18.2	L9	l
J011049.18+192000.1	9.1	M8	w
J013525.38+020518.2	17.7	T0 (sl. red)	l
J022721.93+235654.3	19.4	L9	n, l
J030119.39−231921.1	20.5	T1 (sl. blue)	n, l
J030919.70−501614.2	T7-T9[d]	T7	n, l
J031627.79+265027.5	19.0	T3	l
J032309.12−590751.0	26.2	T7	n, l, s
J032838.73+015517.7	18.5	L5 (blue)	l
J033346.88+385152.6	11.6	M8	s
J034409.71+013641.5	19.1	L8	l
J034858.75−562017.8	22.6	T3	n, l
J041353.96−202320.3	17.7	L5 (blue)	g
J041743.13+241506.3	23.7	T6	n, l
J053424.45+165255.0	15.4	L2 (pec)	n
J054455.54+063940.3	10.3	M9	n
J061429.77+383337.5	10.3	M9	n
J062858.69+345249.2	17.2	L4	l
J063552.52+514820.4	17.4	T0	l
J084254.56−061023.7	22.7	T4	l, n
J085039.11−022154.3	16.3	sdL7 (red)	n
J085633.87−181546.6	11.6	L1	g
J092453.76+072306.0	5.9	M6	s
J094812.21−290329.5	11.8	sdL1	s
J095230.79−282842.2	5.3	esdM4	s
J101944.62−391151.6	24.0	T3 (blue)	n, l, s
J103534.63−071148.2	17.7	sdL7	l
J111320.39+501010.5	7.0	M4 (blue)	s
J112158.76+004412.3	8.6	M7 (blue)	s
J112859.45+511016.8	14.1	L3	g
J120751.17+302808.9	10.6	M8	s
J121231.97−050750.7	5.4	M7 (sl. blue)	s
J121914.75+081027.0	<5	sdM7	s
J122042.20+620528.3	6.3	sdM7	s
J123513.87−045146.5	5.1	esdM4	s
J124516.66+601607.5	9.4	sdM8.5	s
J133520.09−070849.3	12.3	M7	s
J134359.71+634213.1	10.3	M8	g
J143942.79−110045.4	11.8	sdL1	s
J144056.64−222517.8	9.1	sdM8.5	s
J145645.54−103343.5	10.2	M8 (sl. blue)	g
J145747.55−094719.3	6.5	esdM4	s
J155225.22+095155.5	7.9	sdM7	s
J165057.66−221616.8	5.4	M5	n
J171059.52−180108.7	5.2	M4(blue)	n
J171105.08−275531.7	7.3	M6	n
J171454.88+064349.8	15.0	L2(red)	g
J173551.56−820900.3	24.3	T7	n, l
J180839.55+070021.7	14.7	L1 (blue)	s
J182010.20+202125.8	7.4	sdM8.5	s
J183654.10−135926.2	8.7	M6	n
J191011.03+563429.3	11.6	M8	n
J201252.78+124633.3	6.5	M7 (sl. red)	n
J211157.84−521111.3	19.7	T3	l
J215550.34−195428.4	16.7	L7	g
J221737.41−355242.7	10.3	M5	s
J223444.44−230916.1	17.4	L5	l
J224931.10−162759.6	17.1	L5 (blue)	l
J230743.63+052037.3	11.7	M7	w
J234404.85−250042.2	11.8	M7	s

Notes.
[a] Estimated spectral types are from Schneider et al. (2016). They are numerical spectral types where, for example, M2 = 2, L2 = 12, T2 = 25, etc.
[b] Spectral types as determined by comparing our SpeX Prism spectra with spectral standards. Subdwarf spectral types are denoted by the following abbreviations: sd = subdwarf, d/sd = dwarf/subdwarf, and esd = extreme subdwarf.
[c] Lists which of our follow-up categories an object belonged to: n = nearby, s = subdwarf, l = late-type, g = gap object, and w = poor weather target.
[d] WISE 0309−5016 does not show up in 2MASS, so a precise numerical spectral type could not be determined. Instead, an estimate was made based on the *W1*–*W2* color. See Section 3.4 of Schneider et al. (2016) for details.

25 pc < d < 30 pc: two M dwarfs (WISE 0614+3833 M9 and WISE 1910+5634 M8), two L dwarfs (WISE 0008−2813 L8 and WISE 0227+2356 L9), and six T dwarfs (WISE 0004−1336 T2, WISE 0301−2319 T0 (sl. blue), WISE 0328−5620 T3, WISE 0348−5620 T3, WISE 0635+5148 T0, and WISE 2111-5211 T3). Three of our objects are within 15 pc. All three of these are T dwarfs: (WISE 0309−5016 (13.8 ± 1.69; T7), WISE 1735−8209 (12.4 ± 1.28; T7), and WISE 0417+2415 (11.4 ± 0.96; T6)). Even though it is within 15pc, WISE 0417+2415 has no published parallax. The other two have parallaxes published in Kirkpatrick et al. (2019).

5.2. Late-type Brown Dwarfs

While the stellar mass function in the solar neighborhood is well understood (Bastian et al. 2010), the substellar mass function has proven more difficult to measure for two reasons. First, brown dwarfs cool over time, and thus do not follow a mass–luminosity relation as stars do. Second, as mentioned in Section 5.1, the census of brown dwarfs in the solar neighborhood remains incomplete. The census is most incomplete for the late-type T and Y dwarfs because of their intrinsic faintness. However, these objects are among the most important because it has been shown that they provide the best constraints on the underlying mass function (e.g., Burgasser 2004 and Kirkpatrick et al. 2019).

In an effort to identify new late-type objects in the solar neighborhood, we observed 23 candidate late-type objects (⩾L7) from Schneider et al. (2016). Fourteen of these are T dwarfs, with spectral types ranging from T0 to T7; four are late-type L dwarfs; and one (WISE 1035−0711) is an sdL7. The remaining four were mid-L dwarfs, with spectral types of either L4 or L5. We also discovered three additional late-type objects: WISE 2155−1954 (L7), WISE 0004−1336 (T2), and WISE 0850−0221 (sdL7; red), which were not late-type candidates.

WISE 0004−1336 was one of the objects we observed to fill in gaps in our R.A. coverage (see Section 2). In Schneider et al. (2016) it had an estimated spectral type, based on the available photometry, of L6.9, making it just beyond the L7 cutoff, so it was not listed as one of their late-type candidates. When we observed this object, we found it to have a spectral type of T2.

Table 4
Object Distances

AllWISE Designation	Spectral[a] Type	Schneider 2016[b] Dist (pc)	Our Dist (pc)	*Gaia* Source[c] ID	*Gaia*[d] Dist (pc)	Kirkpatrick 2018[e] Dist (pc)
J000430.66−260402.3	T2 (blue)	⋯	25 ± 2.3	⋯	⋯	⋯
J000458.47−133655.1	T2	⋯	29 ± 2.7	⋯	⋯	⋯
J000536.63−263311.8	T0 (pec)	⋯	31 ± 2.6	⋯	⋯	⋯
J000856.39−281321.7	L8	24–34	29 ± 2.5	⋯	⋯	⋯
J010134.83+033616.0	M7	⋯	92 ± 7.7	2551477793805008256	$86^{+5.8}_{-5.1}$	⋯
J010631.20−231415.1	L9	⋯	36 ± 3.2	⋯	⋯	⋯
J011049.18+192000.1	M8	⋯	59 ± 4.9	2786913366801779968	$51.5^{+0.98}_{-0.95}$	⋯
J013525.38+020518.2	T0 (sl. red)	⋯	25 ± 2.1	⋯	⋯	⋯
J022721.93+235654.3	L9	22–31	28 ± 2.3	⋯	⋯	⋯
J030119.39−231921.1	T1 (sl. blue)	24–33	27 ± 2.3	⋯	⋯	⋯
J030919.70−501614.2	T7	9–13	14 ± 1.8	⋯	⋯	15.0 ± 0.87
J031627.79+265027.5	T3	⋯	22 ± 2.1	⋯	⋯	⋯
J032309.12−590751.0	T7	16–26	19 ± 2.2	⋯	⋯	14.0 ± 0.84
J032838.73+015517.7	L5 (blue)	⋯	47 ± 4.5	⋯	⋯	⋯
J033346.88+385152.6	M8	⋯	104 ± 8.7	236441149397820800	$85^{+8.6}_{-7.2}$	⋯
J034409.71+013641.5	L8	⋯	37 ± 3.5	⋯	⋯	⋯
J034858.75−562017.8	T3	24–33	28 ± 3.0	⋯	⋯	⋯
J041353.96−202320.3	L5 (blue)	⋯	41 ± 3.5	⋯	⋯	⋯
J041743.13+241506.3	T6	13–19	12 ± 1.0	⋯	⋯	⋯
J053424.45+165255.0	L2 (pec)	18–25	33 ± 2.8	3397015189186833408	$28^{+3.6}_{-2.8}$	⋯
J054455.54+063940.3	M9	24–37	35 ± 2.9	3333278694852547328	$31.3^{+0.36}_{-0.35}$	⋯
J061429.77+383337.5	M9	18–27	27 ± 2.2	956200977271782144	$25.2^{+0.24}_{-0.23}$	⋯
J062858.69+345249.2	L4	⋯	40. ± 3.3	⋯	⋯	⋯
J063552.52+514820.4	T0	⋯	29 ± 2.7	⋯	⋯	⋯
J084254.56−061023.7	T4	20–29	21 ± 1.9	⋯	⋯	⋯
J085039.11−022154.3	sdL7 (red)	21–30	24 ± 3.4	⋯	⋯	⋯
J085633.87−181546.6	L1	⋯	64 ± 5.4	5728941156831133952	$56^{+4.0}_{-3.5}$	⋯
J092453.76+072306.0	M6	⋯	140 ± 12	586424457955450496	$118^{+8.3}_{-7.3}$	⋯
J094812.21−290329.5	sdL1	⋯	71 ± 9.8	5656672112963964928	$62^{+2.8}_{-2.6}$	⋯
J095230.79−282842.2	esdM4	⋯	110 ± 15	5464936251656505344	$130.^{+2.6}_{-2.5}$	⋯
J101944.62−391151.6	T3 (blue)	19–28	23 ± 2.0	⋯	⋯	⋯
J103534.63−071148.2	sdL7	⋯	42 ± 6.1	⋯	⋯	⋯
J111320.39+501010.5	M4 (blue)	⋯	140 ± 19[f]	838162769031557888	$181^{+10.4}_{-9.3}$	⋯
J112158.76+004412.3	M7 (blue)	⋯	116 ± 9.9	3798149260432886528	$75^{+8.2}_{-6.7}$	⋯
J112859.45+511016.8	L3	⋯	46 ± 3.8	⋯	⋯	⋯
J120751.17+302808.9	M8	⋯	78 ± 6.5	4014105473115624192	$71^{+3.9}_{-3.5}$	⋯
J121231.97−050750.7	M7 (sl. blue)	⋯	71 ± 6.0	3596616230830390016	$66^{+1.9}_{-1.8}$	⋯
J121914.75+081027.0	sdM7	⋯	120 ± 16	3902112585964749312	$122^{+8.5}_{-7.5}$	⋯
J122042.20+620528.3	sdM7	⋯	88 ± 7.4	1583395326382043392	$113^{+4.3}_{-4.0}$	⋯
J123513.87−045146.5	esdM4	⋯	160 ± 22	3680363115235579904	$156^{+5.2}_{-4.9}$	⋯
J124516.66+601607.5	sdM8.5	⋯	100 ± 14	1579775596664490752	$116^{+4.0}_{-3.7}$	⋯
J133520.09−070849.3	M7	⋯	130 ± 11	3630793763800277376	$100.^{+11}_{-9.4}$	⋯
J134359.71+634213.1	M8	⋯	98 ± 8.3	1665037775596252544	$80.^{+6.8}_{-5.8}$	⋯
J143942.79−110045.4	sdL1	⋯	80. ± 11	6324908688520221568	130^{+47}_{-26}	⋯
J144056.64−222517.8	sdM8.5	⋯	80. ± 11	6278872445902622336	$106^{+4.0}_{-3.8}$	⋯
J145645.54−103343.5	M8 (sl. blue)	⋯	61 ± 5.0	6313890619936907136	$49^{+1.4}_{-1.3}$	⋯
J145747.55−094719.3	esdM4	⋯	140 ± 19	6326026685686833920	$166^{+5.9}_{-5.5}$	⋯
J155225.22+095155.5	sdM7	⋯	130 ± 18	4455454422667645184	130^{+14}_{-12}	⋯
J165057.66−221616.8	M5	22–35	41 ± 6.4	4126600390415016832	$34.7^{+0.12}_{-0.12}$	⋯
J171059.52−180108.7	M4 (blue)	24–37	60 ± 12	4134686886136743552	$44.2^{+0.18}_{-0.17}$	⋯
J171105.08−275531.7	M6	21–34	33 ± 2.8	⋯	⋯	⋯
J171454.88+064349.8	L2 (red)	⋯	56 ± 4.8	⋯	⋯	⋯
J173551.56−820900.3	T7	14–21	13 ± 1.4	⋯	⋯	13.3 ± 0.81
J180839.55+070021.7	L1 (blue)	⋯	79 ± 6.7	⋯	⋯	⋯
J182010.20+202125.8	sdM8.5	⋯	80. ± 11	4528661276939071488	$124^{+3.1}_{-3.0}$	⋯
J183654.10−135926.2	M6	20–31	35 ± 3.0	⋯	⋯	⋯
J191011.03+563429.3	M8	16–23	29 ± 2.4	2141364423410899968	$23.48^{+0.07}_{-0.07}$	⋯
J201252.78+124633.3	M7 (sl. red)	17–26	20. ± 1.7	1803225427774999680	$19.27^{+0.03}_{-0.03}$	⋯
J211157.84−521111.3	T3	⋯	26 ± 2.4	⋯	⋯	⋯
J215550.34−195428.4	L7	⋯	39 ± 3.6	⋯	⋯	⋯

Table 4
(Continued)

AllWISE Designation	Spectral[a] Type	Schneider 2016[b] Dist (pc)	Our Dist (pc)	*Gaia* Source[c] ID	*Gaia*[d] Dist (pc)	Kirkpatrick 2018[e] Dist (pc)
J221737.41−355242.7	M5	⋯	150 ± 24	⋯	⋯	⋯
J223444.44−230916.1	L5	⋯	55 ± 5.2	⋯	⋯	⋯
J224931.10−162759.6	L5 (blue)	⋯	37 ± 3.1	⋯	⋯	⋯
J230743.63+052037.3	M7	⋯	64 ± 5.4	2662702873947256832	$87^{+2.9}_{-2.7}$	⋯
J234404.85−250042.2	M7	⋯	84 ± 7.2	2338610933917661696	$63^{+6.0}_{-5.1}$	⋯

Notes.
[a] Spectral types as determined by comparing our SpeX Prism spectra with spectral standards. Subdwarf spectral types are denoted by the following abbreviations: sd = subdwarf, d/sd = dwarf/subdwarf, and esd = extreme subdwarf.
[b] Only listed for objects that were nearby candidates in the Schneider et al. (2016) survey.
[c] Only listed for objects with matches in *Gaia* DR2.
[d] Taken from Bailer-Jones et al. (2018).
[e] Only listed for three objects, which were included in Kirkpatrick et al. (2019).
[f] This is the distance we calculated, assuming this object is a subdwarf. In the absence of this assumption, the distance would be 260 ± 31 pc.

Three other objects (WISE 0005−2633, WISE 0135+0205, and WISE 0635+5148) also had estimated spectral types, based on photometry, of L7 or earlier, and were classified as T dwarfs based on their spectra. In Schneider et al. (2016), the spectral types for these objects were estimated based on their infrared colors (see the Appendix of Schneider et al. 2016 for details), using available photometry. The colors for early T dwarfs can overlap with the colors of mid- to early-L dwarfs (see Figure 5 in Schneider et al. 2016), which can cause these objects to be mistakenly classified as mid-L dwarfs because of the similarity in color. It is likely that this is why these objects were misclassified as L6 or L7, instead of T dwarfs, and why WISE 0004−2604 missed the cutoff for the late-type objects in Schneider et al. (2016).

5.3. Subdwarfs

While effective temperature is the primary parameter that controls the spectral morphology of brown dwarfs, both surface gravity and metallicity also play a role. Our understanding of the impacts that variations in metallicity have on the emergent spectra of brown dwarfs is still in its infancy because of the paucity of metal-poor L and T dwarfs known; the total number currently stands at 71 (Zhang et al. 2018) which is in stark contrast to the thousands of near-solar-metallicity brown dwarfs known. Identifying new metal-poor brown dwarfs will help us to build a large enough sample to begin inferring trends in spectral morphology within a given spectral type, and will allow us to better examine trends across a larger range of subdwarf types.

We conducted follow-up observations of 24 candidate subdwarfs from Schneider et al. (2016). As described in Section 3.1, we have spectra of 16 M and L subdwarf standards, obtained with IRTF/SpeX, which we used to determine which of our objects were subdwarfs. While this is the first time these have been used as near-infrared subdwarf standards, all had previously been spectral typed as subdwarfs in the optical, as detailed in Table 2. Our subdwarf spectral standards include both sd and esd for the M spectral class, and sd for the L spectral class. The esd have $-1.7 < [Fe/H] \leqslant -1.0$, and the sd have $-1.0 < [Fe/H] \leqslant -0.3$ (Gizis 1997; Zhang et al. 2017). All of our observed objects, both subdwarf candidates and non-subdwarf candidates, were compared against both the subdwarf and non-subdwarf standards during the spectral typing process. Final spectral types were determined based on the best match between each object and all available spectral standards. As can be see in Table 2 and Figure 7, our spectral sequence of subdwarf standards is incomplete, especially for the L subdwarfs. This is due to the fact that, at present, there are very few near-infrared spectral standards for subdwarfs available. We have spectral typed our objects to the best of our ability with the available standards, but, we have likely missed some of the subdwarfs in our sample, as a result of not having standards at those spectral types.

Of the 24 subdwarf candidates we observed, 11 were spectral typed as subdwarfs: six sdM (WISE 1219+018 sdM7, WISE 1220+6205 sdM7, WISE 1245+6016 sdM8.5, WISE 1440−2225 sdM8.5, WISE 1552+0951 sdM7, and WISE 1820+2021 sdM8.5), two sdL (WISE 0948−2903 sdL1 and WISE 1439−1100 sdL1), and three esdM4 (WISE 0952−2828, WISE 1235−0451, and WISE 1457−0947). Ten of the remaining 13 were spectral typed as M dwarfs, with spectral types ranging from M4 to M8, one is an L1 (blue), (WISE 1808+0700) and one is a T7 (WISE 0323−5907). The remaining object, WISE 1019−3911, was spectral typed as a T3 (blue). We also observed two objects that were not subdwarf candidates, but were spectral typed as subdwarfs. Both are L subdwarfs. WISE 0850−0221 is a sdL7 (red) and WISE 1035−0711 is a sdL7. According to Zhang et al. (2018), there are 66 known L subdwarfs. This includes four sdL7s, three sdL5s, and four sdL1. We have discovered two additional sdL7s, two additional sdL1s, and three candidate sdL5s, substantially increasing the number of known L subdwarfs at these spectral types.

Due to enhanced collision-induced H_2 absorption, subdwarfs tend to have suppressed flux in the *H*- and *K*-bands, relative to the *J*-band, causing them to appear bluer in the *H*- and *K*-bands than the field objects of the same spectral class. In addition, they exhibit brightening in the *Y*-band. Among the objects we observed, 11 are blue: four M dwarfs, four L dwarfs, and three T dwarfs. For three of these (WISE 1121+0044, M7 (blue), WISE 1456−1033 M8 (sl. blue), and WISE 1808+0700 L1 (blue)), we have subdwarf spectral standards at those spectral types and so can confirm that, while they are blue, they are not subdwarfs. For the remaining eight, we do not. We believe these objects could be subdwarf candidates, but without subdwarf standards at the corresponding spectral types, we

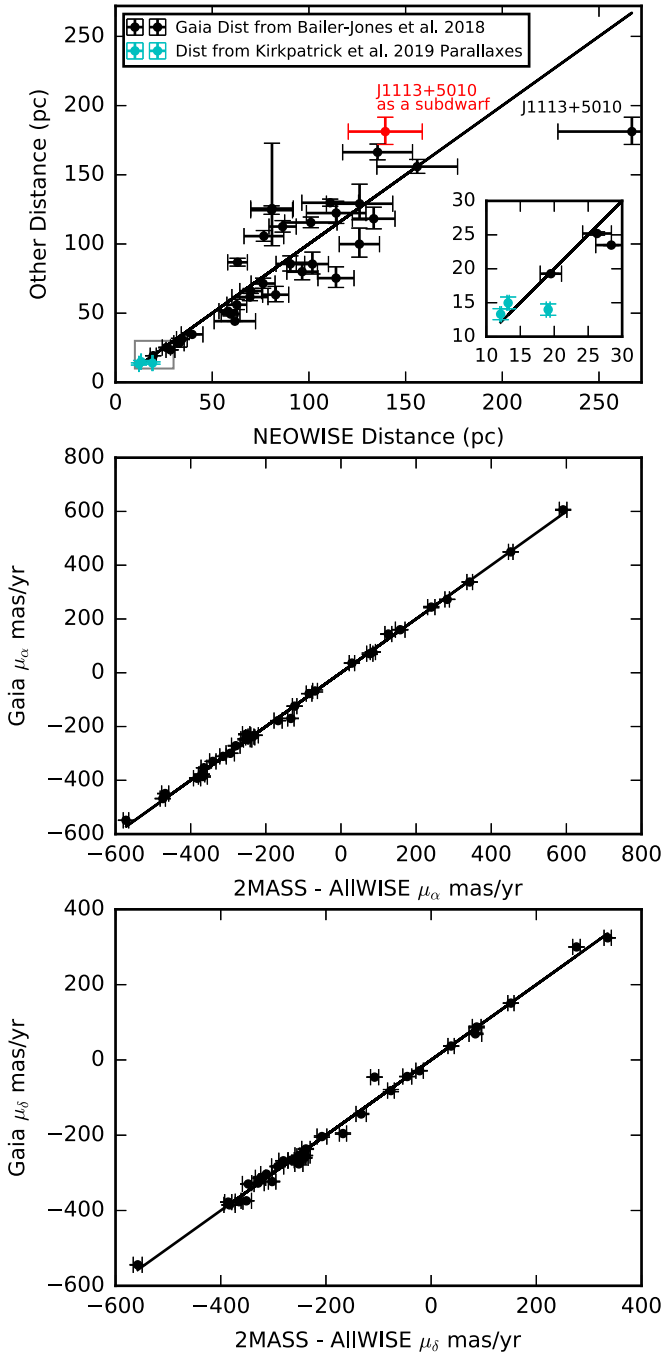

Figure 8. Top panel: comparison of the spectroscopic distances we calculated for each of our objects to the distances from *Gaia*, as determined by Bailer-Jones et al. (2018) and the distances determined from the parallaxes of Kirkpatrick et al. (2019). One of our objects, WISE 1113+5010, shows a large discrepancy between the NEOWISE distance and the *Gaia* distance. We believe this is because it may be a subdwarf (see Section 4.2 for details). We estimated what the spectroscopic distance would be if it was a subdwarf, and that matches up much better with the *Gaia* distance, as show in this figure. Middle and bottom panels: comparison of the NEOWISE proper motions and the *Gaia* proper motions for all objects that appear in *Gaia*. There is good agreement between these for all of our objects.

cannot be certain at this time. We have three new candidate T subdwarfs: WISE 0301−2319 (sdT1), WISE 0004−2604 (sdT2), and WISE 1019−3911 (sdT3); three new candidate sdL5: WISE 0328+0155, WISE 0413−2023, and WISE 2249−1627; and two new candidate sdM4: WISE 1113+5010 and WISE 1710−1801.

Additionally, WISE 0948−2903 (sdL1), WISE 1439−1100 (sdL1), and some of the blue late Ms (e.g., WISE 1212−0507 and WISE 1121+0044) show a triangular *H*-band peak, a feature that is seen in the spectra of young, low-gravity M and L dwarfs and attributed to reduced collision-induced H_2 absorption in low pressure atmospheres (e.g., Rice et al. 2011; Allers & Liu 2013). Aganze et al. (2016) analyzed this feature while studying the d/sdM7 GJ 660.1B which has [Fe/H] = −0.63 ± 0.06, and found that this feature is also indicative of subsolar metallicity. The presence of this feature in our spectra supports the classification of WISE 0948−2903 and WISE 1439−1100 as subdwarfs, and suggests that the blue M dwarfs may also have subsolar metallicities.

Among our discoveries, we find three new T subdwarf candidates all with distances around 25 pc. One of these, WISE 1019−3911, was listed as a candidate in all three categories. Based on the estimates from Schneider et al. (2016), WISE 1019−3911 was expected to be a T dwarf, with an estimated spectral type based on photometry of T4, an estimated distance of 19–28 pc, and was also a subdwarf candidate. We observed it using CTIO/ARCoIRIS, and spectral typed it as a T3 (blue) with a distance of 25.1 ± 0.32 pc. The other two, WISE 0004−2604 and WISE 0301−2319, were not subdwarf candidates. WISE 0004−2604 was a late-type candidate with an estimated spectral type, based on photometry of T0.5, and WISE 0301−2319 was a nearby late-type candidate with an estimated spectral type, based on photometry, of T0.5, and an estimated distance of 24–33 pc. We observed both of them with IRTF/SpeX, and typed WISE 0004−2604 as T2 (blue) with a distance of 25 ± 2.3 pc and WISE 0301−2319 as T1 (sl. blue) with a distance of 27 ± 2.3 pc.

If confirmed, these three objects would more than double the number of known early-type T subdwarfs. To date, only two early-type T subdwarfs are known: the sdT0 WISE 071121.36−573634.2 discovered by Kellogg et al. (2018) as part of the follow-up for the AllWISE2 motion survey (Kirkpatrick et al. 2016), and the sdT1.5 WISE 210529.08−623558.7 discovered by Luhman & Sheppard (2014) as part of an analysis of high proper motion objects from the *WISE* survey. In addition, there are three published late-type T subdwarfs: the sdT5.5 HIP 73786B, a common proper motion companion to the metal-poor K-star HIP 73786 discovered by Murray et al. (2011) using data from the United Kingdom InfraRed Telescope Infrared Deep Sky Survey (UKIDSS); the sdT6.5 ULAS J131610.28+075553.0 discovered by Burningham et al. (2014) in the UKIDSS Large Area Survey; and the sdT8 WISE J200520.38+542433.9, a companion to the sdM1.5 Wolf 1130, discovered by Mace et al. (2013) using photometry from 2MASS, WISE, and other telescopes. Although it was not initially designated as a T subdwarf, Burgasser et al. (2006) showed that the peculiar T6 dwarf 2MASS 0937+2931 has a subsolar metallicity and has a spectral morphology consistent with other T subdwarfs. In addition, Zhang et al. (2019) report 38 metal-poor T dwarfs that show suppressed *K*-band flux in their spectra, which they believe might be T subdwarfs. All of these have spectral types of T5 or later.

As discussed above, there are gaps in our sequence of subdwarf spectral standards. We do have spectra of several subdwarf candidates at these missing spectral types including two candidate sdM4: WISE 1113+5010 and WISE 1710−1801; three new candidate sdL5: WISE 0328+0155, WISE 0413−2023, and WISE 2249−1627; and three new candidate

Table 5
Photometry, Proper Motions, Spectral Types, and Tangential Velocities of All Observed Objects

AllWISE Designation	2MASS J (mag)	2MASS H (mag)	2MASS K_s (mag)	*WISE* $W1$ (mag)	*WISE* $W2$ (mag)	μ_α (mas yr^{-1})	μ_δ (mas yr^{-1})	$v_{\rm tan}$ km s^{-1}	Spectral Type
J000430.66−260402.3	16.487 ± 0.133	15.587 ± 0.129	>15.523	15.211 ± 0.038	14.127 ± 0.044	11.9 ± 15.3	−229.6 ± 13.8	27 ± 2.9	T2 (blue)
J000458.47−133655.1	16.841 ± 0.171	16.120 ± 0.207	>15.410	15.120 ± 0.037	14.457 ± 0.056	431.3 ± 21.8	−37.4 ± 20.3	59 ± 6.3	T2
J000536.63−263311.8	17.171 ± 0.225	15.849 ± 0.165	15.191 ± 0.154	14.924 ± 0.033	14.261 ± 0.047	384.0 ± 22.8	39.8 ± 20.5	56 ± 5.8	T0 (pec)
J000856.39−281321.7	16.727 ± 0.137	15.664 ± 0.139	15.049 ± 0.131	14.119 ± 0.027	13.636 ± 0.037	284.3 ± 16.0	−54.7 ± 13.6	40 ± 4.0	L8
J010134.83+033616.0	15.418 ± 0.052	14.650 ± 0.066	14.300 ± 0.069	14.206 ± 0.029	13.941 ± 0.039	591.3 ± 10.0	−557.8 ± 8.5	360 ± 30.	M7
J010631.20−231415.1	17.338 ± 0.235	16.115 ± 0.204	15.683 ± 0.241	14.899 ± 0.033	14.417 ± 0.049	−271.5 ± 24.8	−201.6 ± 23.2	57 ± 6.6	L9
J011049.18+192000.1	14.708 ± 0.032	14.142 ± 0.038	13.827 ± 0.05	13.467 ± 0.025	13.147 ± 0.03	451.9 ± 6.0	38.0 ± 6.0	130 ± 10.	M8
J013525.38+020518.2	16.622 ± 0.129	15.481 ± 0.104	15.123 ± 0.117	14.283 ± 0.028	13.883 ± 0.04	102.9 ± 16.2	−494.1 ± 15.2	60 ± 5.4	T0 (sl. red)
J022721.93+235654.3	16.663 ± 0.135	15.647 ± 0.105	15.270 ± 0.155	14.304 ± 0.027	13.690 ± 0.035	310.0 ± 15.2	−139.0 ± 13.6	44 ± 4.2	L9
J030119.39−231921.1	16.635 ± 0.144	15.800 ± 0.158	15.579 ± 0.234	14.829 ± 0.03	14.036 ± 0.036	263.7 ± 27.9	−141.4 ± 22.9	38 ± 4.7	T1 (sl. blue)
J030919.70−501614.2[a]	…	…	…	16.465 ± 0.057	13.631 ± 0.031	…	…	…	T7
J031627.79+265027.5	16.585 ± 0.149	15.592 ± 0.159	>15.159	14.980 ± 0.035	13.934 ± 0.04	209.0 ± 22.5	−15.6 ± 20.2	22 ± 3.1	T3
J032309.12−590751.0	16.881 ± 0.189[b]	>16.669	>16.262	16.804 ± 0.065	14.529 ± 0.039	542.9 ± 24.0	476.7 ± 21.4	66 ± 7.6	T7
J032838.73+015517.7	16.504 ± 0.172	>16.598	15.202 ± 0.182	14.645 ± 0.031	14.327 ± 0.053	190.8 ± 22.7	−233.2 ± 19.0	66 ± 7.8	L5 (blue)
J033346.88+385152.6	16.073 ± 0.071	15.276 ± 0.082	15.000 ± 0.118	14.654 ± 0.03	14.350 ± 0.047	240.4 ± 9.7	−324.3 ± 9.8	200 ± 17	M8
J034409.71+013641.5	>17.024	15.949 ± 0.198	15.549 ± 0.232	14.647 ± 0.034	14.183 ± 0.05	−72.0 ± 31.2	−286.6 ± 30.3	51 ± 7.2	L8
J034858.75−562017.8	16.652 ± 0.151	>15.940	>15.517	14.233 ± 0.028	13.919 ± 0.036	169.7 ± 18.0	206.6 ± 16.3	36 ± 4.3	T3
J041353.96−202320.3	16.392 ± 0.111	15.444 ± 0.116	15.132 ± 0.174	14.233 ± 0.028	13.919 ± 0.036	−41.8 ± 15.0	−349.9 ± 14	20 ± 2.7	L5 (blue)
J041743.13+241506.3	15.766 ± 0.069	15.654 ± 0.136	15.450 ± 0.167	14.520 ± 0.032	13.374 ± 0.035	403.6 ± 10.1	−489.8 ± 10.2	35 ± 3.2	T6
J053424.45+165255.0	15.445 ± 0.041	14.385 ± 0.037	13.572 ± 0.041	12.969 ± 0.024	12.575 ± 0.025	−69.0 ± 6.4	−76.4 ± 6.4	16 ± 1.7	L2 (pec)
J054455.54+063940.3	14.039 ± 0.032	13.286 ± 0.028	12.795 ± 0.033	12.494 ± 0.024	12.265 ± 0.025	157.7 ± 12.8	−329.2 ± 11.9	61 ± 5.3	M9
J061429.77+383337.5	13.523 ± 0.024	12.748 ± 0.029	12.251 ± 0.02	11.848 ± 0.024	11.619 ± 0.022	84.9 ± 6.9	−385.8 ± 6.8	50 ± 4.2	M9
J062858.69+345249.2	15.957 ± 0.084	15.265 ± 0.089	14.706 ± 0.084	13.923 ± 0.027	13.615 ± 0.039	8.2 ± 7.4	−286.5 ± 7.4	54 ± 4.7	L4
J063552.52+514820.4	>16.680	15.504 ± 0.144	15.416 ± 0.180	14.610 ± 0.031	14.294 ± 0.046	−121.1 ± 18.9	−243.2 ± 17.3	37 ± 4.2	T0
J084254.56−061023.7	16.040 ± 0.076	15.680 ± 0.111	>15.127	15.444 ± 0.041	14.086 ± 0.041	−375.9 ± 14.9	−45.0 ± 14.4	37 ± 3.7	T4
J085039.11−022154.3	15.443 ± 0.044	14.504 ± 0.041	14.100 ± 0.059	13.408 ± 0.025	13.100 ± 0.028	−392.0 ± 6.7	−132.1 ± 6.7	47 ± 6.6	sdL7 (red)
J085633.87−181546.6	15.828 ± 0.071	15.252 ± 0.094	14.473 ± 0.095	14.350 ± 0.029	14.178 ± 0.043	76.7 ± 8.3	−251.5 ± 7.7	80 ± 7.0	L1
J092453.76+072306.0	15.752 ± 0.083	15.272 ± 0.094	14.754 ± 0.112	14.722 ± 0.032	14.488 ± 0.054	−248.4 ± 11.1	−383.2 ± 10.7	290 ± 27	M6
J094812.21−290329.5	15.542 ± 0.056	15.019 ± 0.066	14.848 ± 0.122	14.332 ± 0.028	13.962 ± 0.03	−370.3 ± 7.8	−238.0 ± 8.0	150 ± 20	sdL1
J095230.79−282842.2	14.942 ± 0.043	14.451 ± 0.041	14.050 ± 0.058	13.934 ± 0.027	13.651 ± 0.034	−572.2 ± 7.2	276.3 ± 7.2	340 ± 46	esdM4
J101944.62−391151.6	16.027 ± 0.096	15.766 ± 0.125	15.727 ± 0.267	15.645 ± 0.044	14.217 ± 0.042	−472.2 ± 28.0	222.7 ± 26.4	58 ± 5.9	T3 (blue)
J103534.63−071148.2	16.393 ± 0.094	15.843 ± 0.128	15.145 ± 0.141	14.381 ± 0.029	14.085 ± 0.045	−375.5 ± 18.9	−28.4 ± 15.8	80 ± 11.	sdL7
J111320.39+501010.5	15.506 ± 0.06	14.804 ± 0.086	14.898 ± 0.113	14.603 ± 0.029	14.411 ± 0.046	−167.3 ± 10.8	−313.2 ± 10.9	330 ± 54	M4 (blue)
J112158.76+004412.3	15.961 ± 0.077	15.256 ± 0.075	14.877 ± 0.133	14.715 ± 0.033	14.297 ± 0.047	−383.0 ± 9.5	−133.0 ± 9.8	224 ± 20	M7 (blue)
J112859.45+511016.8	16.189 ± 0.069	15.110 ± 0.078	14.490 ± 0.069	13.944 ± 0.026	13.692 ± 0.032	−117.7 ± 9.0	−321.9 ± 9.1	74 ± 6.4	L3
J120751.17+302808.9	15.253 ± 0.051	14.799 ± 0.071	14.467 ± 0.077	14.046 ± 0.027	13.713 ± 0.033	126.1 ± 9.1	−241.1 ± 7.2	100 ± 8.9	M8
J121231.97−050750.7	14.676 ± 0.032	14.201 ± 0.028	13.845 ± 0.049	13.663 ± 0.028	13.366 ± 0.033	−474.2 ± 7.0	−21.9 ± 7.1	160 ± 13	M7 (sl. blue)
J121914.75+081027.0	15.780 ± 0.085	15.076 ± 0.096	14.979 ± 0.148	14.796 ± 0.034	14.567 ± 0.059	−279.9 ± 11.4	−347.7 ± 11.1	250 ± 34	sdM7
J122042.20+620528.3	15.433 ± 0.054	14.830 ± 0.062	14.730 ± 0.086	14.487 ± 0.029	14.152 ± 0.034	−467.9 ± 9.4	−280.9 ± 8.7	230 ± 19	sdM7
J123513.87−045146.5	15.681 ± 0.072	15.195 ± 0.083	15.029 ± 0.142	14.808 ± 0.033	14.535 ± 0.057	−230.0 ± 10.1	−351.4 ± 9.9	317 ± 44	esdM4
J124516.66+601607.5	15.663 ± 0.058	15.297 ± 0.104	15.086 ± 0.116	14.711 ± 0.028	14.502 ± 0.043	−294.7 ± 11.1	−239.8 ± 9.7	190 ± 26	sdM8.5
J133520.09−070849.3	16.336 ± 0.097	15.365 ± 0.09	14.989 ± 0.134	14.932 ± 0.034	14.565 ± 0.056	−367.5 ± 11.9	84.1 ± 12.0	230 ± 21	M7
J134359.71+634213.1	16.004 ± 0.085	15.202 ± 0.106	14.795 ± 0.096	14.476 ± 0.025	14.262 ± 0.033	−254.0 ± 12.4	86.7 ± 8.3	130 ± 12	M8
J143942.79−110045.4	15.837 ± 0.086	15.365 ± 0.098	15.038 ± 0.145	14.586 ± 0.03	14.213 ± 0.043	−252.3 ± 9.8	−207.6 ± 9.3	130 ± 18	sdL1
J144056.64−222517.8	15.077 ± 0.05	14.688 ± 0.058	14.453 ± 0.087	14.108 ± 0.029	13.780 ± 0.042	−239.5 ± 7.8	−247.3 ± 7.9	130 ± 18	sdM8.5
J145645.54−103343.5	14.856 ± 0.049	14.197 ± 0.055	13.849 ± 0.044	13.467 ± 0.026	13.166 ± 0.031	29.2 ± 7.1	−302.3 ± 7.1	87 ± 7.6	M8 (sl. blue)
J145747.55−094719.3	15.331 ± 0.048	14.930 ± 0.063	14.688 ± 0.097	14.377 ± 0.029	14.205 ± 0.048	−313.9 ± 8.6	−250.9 ± 8.0	260 ± 36	esdM4

Table 5
(Continued)

AllWISE Designation	2MASS J (mag)	2MASS H (mag)	2MASS K_s (mag)	*WISE W*1 (mag)	*WISE W*2 (mag)	μ_α (mas yr^{-1})	μ_δ (mas yr^{-1})	$v_{\rm tan}$ km s^{-1}	Spectral Type
J155225.22+095155.5	15.923 ± 0.088	15.360 ± 0.082	15.164 ± 0.147	14.756 ± 0.03	14.554 ± 0.054	−241.5 ± 12.1	−291.8 ± 11.5	230 ± 33	sdM7
J165057.66−221616.8	12.218 ± 0.024	11.679 ± 0.027	11.332 ± 0.026	11.122 ± 0.023	10.929 ± 0.021	−123.3 ± 5.9	−266.1 ± 5.9	57 ± 8.9	M5
J171059.52−180108.7	12.314 ± 0.027	11.800 ± 0.025	>11.509	11.208 ± 0.024	11.027 ± 0.021	−84.8 ± 7.5	−365.1 ± 7.3	110 ± 22	M4(blue)
J171105.08−275531.7	12.760 ± 0.033	12.190 ± 0.036	11.853 ± 0.037	11.456 ± 0.024	11.315 ± 0.023	−169.0 ± 6.2	−373.0 ± 6.1	63 ± 5.6	M6
J171454.88+064349.8	16.617 ± 0.132	15.467 ± 0.114	14.594 ± 0.089	14.066 ± 0.026	13.782 ± 0.036	−83.2 ± 10.6	−322.0 ± 10.6	88 ± 8.0	L2 (red)
J173551.56−820900.3	16.393 ± 0.14	>15.949	>15.996	15.570 ± 0.036	13.723 ± 0.029	−232.3 ± 16.3	−253.4 ± 15.5	21 ± 2.4	T7
J180839.55+070021.7	16.125 ± 0.104	15.731 ± 0.143	15.338 ± 0.169	14.821 ± 0.034	14.497 ± 0.055	−235.1 ± 21.4	−177.8 ± 19.8	110 ± 12	L1 (blue)
J182010.20+202125.8	15.188 ± 0.051	14.802 ± 0.071	14.606 ± 0.076	14.409 ± 0.03	14.174 ± 0.04	−341.1 ± 8.5	−45.4 ± 8.5	130 ± 19	sdM8.5
J183654.10−135926.2	12.997 ± 0.024	12.433 ± 0.023	12.031 ± 0.019	11.542 ± 0.028	11.480 ± 0.029	−21.2 ± 6.5	−368.2 ± 6.6	61 ± 5.3	M6
J191011.03+563429.3	13.281 ± 0.027	12.654 ± 0.033	12.231 ± 0.026	11.825 ± 0.022	11.549 ± 0.021	−364.6 ± 7.8	335.7 ± 6.9	68 ± 5.7	M8
J201252.78+124633.3	12.040 ± 0.021	11.425 ± 0.021	11.035 ± 0.018	10.796 ± 0.023	10.596 ± 0.02	282.7 ± 6.0	151.7 ± 5.9	30 ± 2.6	M7 (sl. red)
J211157.84−521111.3	16.563 ± 0.166	15.923 ± 0.212	>15.252	15.371 ± 0.039	14.308 ± 0.043	−227.2 ± 28.5	87.3 ± 26.7	30 ± 4.4	T3
J215550.34−195428.4	>16.978	15.971 ± 0.146	15.277 ± 0.142	14.552 ± 0.03	14.172 ± 0.044	−34.0 ± 16.8	−352.7 ± 16.1	66 ± 6.7	L7
J221737.41−355242.7	14.874 ± 0.051	14.540 ± 0.068	14.236 ± 0.066	13.816 ± 0.025	13.573 ± 0.032	49.0 ± 7.1	−304.9 ± 7.1	220 ± 35	M5
J223444.44−230916.1	15.262 ± 0.086	14.831 ± 0.11	14.082 ± 0.027	13.745 ± 0.037	16.121 ± 0.085	408.9 ± 24.8	−26.8 ± 22.5	110 ± 12	L5
J224931.10−162759.6	17.328 ± 0.228	16.284 ± 0.24	>14.679	14.843 ± 0.034	14.368 ± 0.053	374.5 ± 8.8	126.2 ± 8.7	69 ± 6.0	L7
J230743.63+052037.3	14.741 ± 0.038	14.058 ± 0.027	13.763 ± 0.039	13.159 ± 0.024	13.032 ± 0.028	−133.3 ± 8.5	−107.5 ± 7.7	52 ± 5.0	M7
J234404.85−250042.2	15.253 ± 0.056	14.634 ± 0.079	14.392 ± 0.083	13.881 ± 0.027	13.563 ± 0.034	342.7 ± 7.5	−167.6 ± 6.8	150 ± 13	M7

Notes.
[a] WISE 030919.70−501614.2 does not show up in 2MASS, and therefore does not have a 2MASS–AllWISE proper motion, and also does not have a calculated $v_{\rm tan}$.
[b] The 2MASS J-band photometry for WISE 032309.12−590751.0 was taken from the 2MASS reject table.

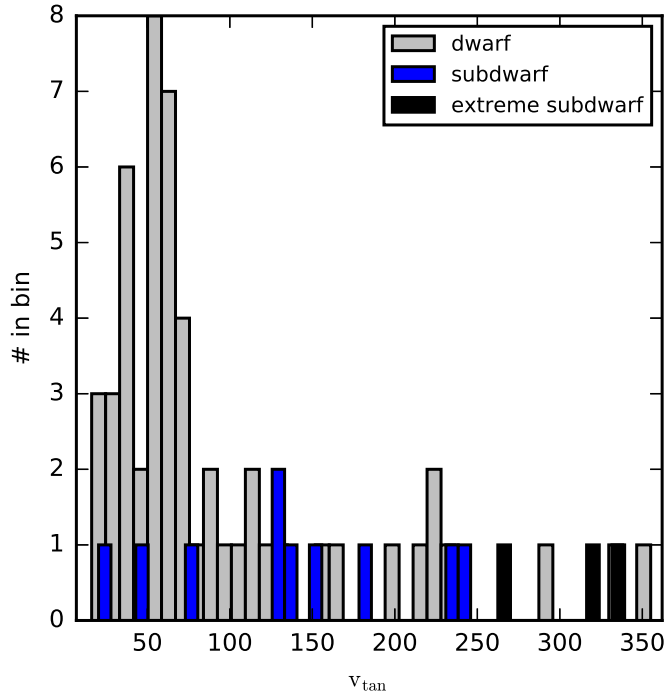

Figure 9. Distribution of tangential velocities for our objects.

T subdwarfs: WISE 0301−2319 (sdT1), WISE 0004−2604 (sdT2), and WISE 1019−3911 (sdT3). These objects could potentially be used to fill in these holes in the sequence. This is beyond the scope of this work but, in the future these spectra could aid in the construction of a more complete classification scheme for subdwarfs.

We also calculated tangential velocities and their uncertainties for each of our objects, using a Monte Carlo approach to properly account for the uncertainties in the distances and proper motions. Normal distributions were constructed for μ_α, μ_δ, and distance, using their uncertainties. Values for each were randomly drawn from those distributions and used to calculate $v_{\rm tan}$. This process was repeated 10,000 times, and the resulting distribution was fit to determine $v_{\rm tan}$ and its uncertainty for each object. These values are reported in Table 5 and plotted in Figure 9. In Dupuy & Liu (2012), they computed the membership probability as a function of tangential velocity for the thin-disk, thick-disk, and halo populations. Based on the results plotted in Figure 31 of that paper, we define the $v_{\rm tan}$ values for these regions as follows: halo $v_{\rm tan} \gtrsim 250$ km s^{-1}; thick disk 100 km s^{-1} $\lesssim v_{\rm tan} \gtrsim 250$ km s^{-1}; and thin disk $v_{\rm tan} \lesssim 100$ km s^{-1}. All three of the extreme subdwarfs in our sample have $v_{\rm tan} \gtrsim 250$ km s^{-1}, putting them in the halo, as expected of older, lower metallicity subdwarfs, which tend to be kinematically associated with the halo population. The dwarfs in our sample are likely clustered in the thin disk, though it is likely some are also in the thick disk. The subdwarfs in our sample are likely distributed throughout the thick and thin disk. Three of our dwarfs have tangential velocities that place them in the halo: WISE 0101+0336 (355.0 ± 30.1 km s^{-1}), WISE 0924+0723 (290 ± 26 km s^{-1}), and WISE 1113+5010 (460 ± 76 km s^{-1}). The velocity of WISE 1113+5010 is approaching the escape velocity of the Galaxy, which is $v_{\rm tan} = 528^{+24}_{-25}$ km s^{-1} at the Sun's position (Deason et al. 2019).

This paper includes data gathered from the 6.5 m *Magellan* Telescopes located at Las Campanas Observatory, Chile, and is based in part on observations from Cerro Tololo Inter-American Observatory, National Optical Astronomy Observatory (NOAO Prop. ID 2016B-0003; PI: A. Schneider), which is operated by the Association of Universities for Research in Astronomy (AURA) under a cooperative agreement with the National Science Foundation. This publication makes use of data products from the *Wide-field Infrared Survey Explorer*, which is a joint project of the University of California, Los Angeles, and the Jet Propulsion Laboratory/California Institute of Technology, and NEOWISE which is a project of the Jet Propulsion Laboratory/California Institute of Technology. *WISE* and NEOWISE are funded by the National Aeronautics and Space Administration. This research has benefited from the M, L, T and Y dwarf compendium hosted at DwarfArchives.org. This research made use of the SIMBAD database, operated at CDS, Strasbourg, France.

Facilities: IRTF(SpeX), *Magellan*:Baade(FIRE), Blanco (ARCoIRIS).

Software: Spextool (Vacca et al. 2003; Cushing et al. 2004).

ORCID iDs

Jennifer J. Greco https://orcid.org/0000-0002-4649-1568
Adam C. Schneider https://orcid.org/0000-0002-6294-5937
Michael C. Cushing https://orcid.org/0000-0001-7780-3352
J. Davy Kirkpatrick https://orcid.org/0000-0003-4269-260X
Adam J. Burgasser https://orcid.org/0000-0002-6523-9536

References

Aganze, C., Burgasser, A. J., Faherty, J. K., et al. 2016, AJ, 151, 46
Allers, K. N., & Liu, M. C. 2013, ApJ, 772, 79
Bailer-Jones, C. A. L., Rybizki, J., Fouesneau, M., Mantelet, G., & Andrae, R. 2018, AJ, 156, 58
Bastian, N., Covey, K. R., & Meyer, M. R. 2010, ARA&A, 48, 339
Best, W. M. J., Liu, M. C., Magnier, E. A., et al. 2015, ApJ, 814, 118
Burgasser, A. J. 2004, ApJS, 155, 191
Burgasser, A. J., Burrows, A., & Kirkpatrick, J. D. 2006, ApJ, 639, 1095
Burgasser, A. J., Cruz, K. L., & Kirkpatrick, J. D. 2007, ApJ, 657, 494
Burgasser, A. J., Gillon, M., Melis, C., et al. 2015, AJ, 149, 104
Burgasser, A. J., & Kirkpatrick, J. D. 2006, ApJ, 645, 1485
Burgasser, A. J., McElwain, M. W., Kirkpatrick, J. D., et al. 2004, AJ, 127, 2856
Burgasser, A. J., Witte, S., Helling, C., et al. 2009, ApJ, 697, 148
Burningham, B., Smith, L., Cardoso, C. V., et al. 2014, MNRAS, 440, 359
Cushing, M. C., Kirkpatrick, J. D., Gelino, C. R., et al. 2011, ApJ, 743, 50
Cushing, M. C., Vacca, W. D., & Rayner, J. T. 2004, PASP, 116, 362
Cutri, R. M. E. 2014, yCat, 2328
Deason, A. J., Fattahi, A., Belokurov, V., et al. 2019, MNRAS, 485, 3514
Dupuy, T. J., & Liu, M. C. 2012, ApJS, 201, 19
Fazio, G. G., Hora, J. L., Allen, L. E., et al. 2004, ApJS, 154, 10
Gizis, J. E. 1997, AJ, 113, 806
Gizis, J. E., & Reid, I. N. 1999, AJ, 117, 508
Henry, T. J., Jao, W.-C., Winters, J. G., et al. 2018, AJ, 155, 265
Kellogg, K., Kirkpatrick, J. D., Metchev, S., Gagné, J., & Faherty, J. K. 2018, AJ, 155, 87
Kirkpatrick, J. D., Gelino, C. R., Cushing, M. C., et al. 2012, ApJ, 753, 156
Kirkpatrick, J. D., Kellogg, K., Schneider, A. C., et al. 2016, ApJS, 224, 36
Kirkpatrick, J. D., Looper, D. L., Burgasser, A. J., et al. 2010, ApJS, 190, 100
Kirkpatrick, J. D., Martin, E. C., Smart, R. L., et al. 2019, ApJS, 240, 19
Kirkpatrick, J. D., Schneider, A., Fajardo-Acosta, S., et al. 2014, ApJ, 783, 122
Luhman, K. L. 2013, ApJL, 767, L1
Luhman, K. L. 2014a, ApJL, 786, L18
Luhman, K. L. 2014b, ApJ, 781, 4
Luhman, K. L., & Sheppard, S. S. 2014, ApJ, 787, 126
Mace, G. N., Kirkpatrick, J. D., Cushing, M. C., et al. 2013, ApJ, 777, 36
Mainzer, A., Bauer, J., Cutri, R. M., et al. 2014, ApJ, 792, 30

Mainzer, A., Bauer, J., Grav, T., et al. 2011, ApJ, 731, 53
Mamajek, E. E., Barenfeld, S. A., Ivanov, V. D., et al. 2015, ApJL, 800, L17
Murray, D. N., Burningham, B., Jones, H. R. A., et al. 2011, MNRAS, 414, 575
Rayner, J. T., Toomey, D. W., Onaka, P. M., et al. 2003, PASP, 115, 362
Reid, I. N., & Gizis, J. E. 2005, PASP, 117, 676
Riaz, B., Gizis, J. E., & Samaddar, D. 2008, ApJ, 672, 1153
Rice, E. L., Faherty, J. K., Cruz, K., et al. 2011, in ASP Conf. Ser. 448, 16th Cambridge Workshop on Cool Stars, Stellar Systems, and the Sun, ed. C. Johns-Krull, M. K. Browning, & A. A. West (San Francisco, CA: ASP), 481
Robert, J., Gagné, J., Artigau, É, et al. 2016, ApJ, 830, 144
Ruiz, M. T., & Anguita, C. 1993, AJ, 105, 614
Schneider, A. C., Greco, J., Cushing, M. C., et al. 2016, ApJ, 817, 112
Scholz, R.-D. 2014, A&A, 561, A113
Scholz, R.-D., Lehmann, I., Matute, I., & Zinnecker, H. 2004, A&A, 425, 519
Schweitzer, A., Scholz, R.-D., Stauffer, J., Irwin, M., & McCaughrean, M. J. 1999, A&A, 350, L62
Simcoe, R. A., Burgasser, A. J., Schechter, P. L., et al. 2013, PASP, 125, 270
Tinney, C. G., Kirkpatrick, J. D., Faherty, J. K., et al. 2018, ApJS, 236, 28
Vacca, W. D., Cushing, M. C., & Rayner, J. T. 2003, PASP, 115, 389
Werner, M. W., Roellig, T. L., Low, F. J., et al. 2004, ApJS, 154, 1
Wright, E. L., Eisenhardt, P. R. M., Mainzer, A. K., et al. 2010, AJ, 140, 1868
Zhang, Z. H., Burgasser, A. J., Gálvez-Ortiz, M. C., et al. 2019, MNRAS, 486, 1260
Zhang, Z. H., Galvez-Ortiz, M. C., Pinfield, D. J., et al. 2018, MNRAS, 480, 5447
Zhang, Z. H., Pinfield, D. J., Burningham, B., et al. 2013, MNRAS, 434, 1005
Zhang, Z. H., Pinfield, D. J., Gálvez-Ortiz, M. C., et al. 2017, MNRAS, 464, 3040